

Geochemical characteristics and magma fertility for the Jurassic arc rocks in the Gangdese belt, Tibet

Xilian Chen^{a,b,c}, Huaying Liang^{a,*}, Jian Zhang^{a,c}, Paul Sotiriou^d, Wenting Huang^a, Long Ren^{a,c}, Le Zhang^{c,e}, Yinqiao Zou^{a,c}

^a Key Laboratory of Mineralogy and Metallogeny, Guangzhou Institute of Geochemistry, Chinese Academy of Sciences, 511 Kehua Street, Wushan, Guangzhou 510640, China

^b State Key Laboratory of Nuclear Resources and Environment, East China University of Technology, Nanchang 330013, China

^c University of Chinese Academy of Sciences, Beijing 100049, China

^d Department of Earth and Environmental Sciences, University of Windsor, Windsor, Ontario N9B 3P4, Canada

^e State Key Laboratory of Isotope Geochemistry, Guangzhou Institute of Geochemistry, Chinese Academy of Sciences, Guangzhou 510640, China



ARTICLE INFO

Keywords:

Jurassic magmatic rocks
Geochemical variation
Porphyry Cu mineralization
The Gangdese belt

ABSTRACT

Jurassic arc magmatic rocks are widely distributed along the Gangdese belt, southern Tibet, however, only one Jurassic arc-related porphyry Cu deposit (the Xietongmen deposit) has been found. The Jurassic arc magma fertility needs to be further constrained in order to understand the rarity of arc-related porphyry Cu deposits in this belt. This paper seeks to combine new data on the Jurassic granitoid rocks with all published data on the Jurassic magmatic rocks in the Gangdese belt to comprehensively explore their geochemical variation and magma fertility. Our new data show that the Jurassic granitoid rocks have zircon U–Pb ages of 171.6 ± 1.1 Ma to 195.3 ± 1.3 Ma. These Jurassic granitoids are calc-alkaline series with SiO_2 contents of 59.4 to 70.7 wt%, Mg# values of 35 to 53, and A/CNK values of 0.72–1.25 (mainly < 1.1). They show enrichment in LREE and LILEs, depletion in HREE and HFSEs, and have depleted Sr–Nd–Hf isotopic compositions. These characteristics suggest that they were probably formed by the interaction of mantle-wedge-derived basaltic magmas with juvenile lower crust. The compiled Jurassic magmatic rocks in the Gangdese belt generally contain amphibole and a mineral assemblage of titanite + magnetite + quartz. These rocks have high whole-rock Sr/Y (> 20), V/Sc ratios (> 8) and high zircon $\text{Eu}_N/\text{Eu}_N^*$ (> 0.3), $\text{Ce}^{4+}/\text{Ce}^{3+}$ ratios (> 300), and low titanium-in-zircon temperatures ($< 750^\circ\text{C}$), except for some localized areas that deviate from the main trend. These features indicate that nearly all Jurassic arc magmas in the Gangdese belt are water-rich and oxidized, which are fertile for porphyry Cu mineralization. The rarity of the Jurassic subduction-related porphyry Cu deposits may result from subsequent erosion or insufficient exploration.

1. Introduction

Porphyry Cu (\pm Mo \pm Au) deposits are typically associated with hydrous and oxidized magmas that formed in both arc and collisional settings (Cooke et al., 2005; Sillitoe, 2010; Hou et al., 2015a,b; Sun et al., 2013, 2015). The lack of generation of these fertile magmas will reduce the potential for ore formation significantly, and even lead to large-scale barren systems (Richards, 2013, 2015). Therefore, assessment of magma fertility through mineral assemblage observations, whole rock geochemistry and mineral compositions is a key step to help evaluate the mineralization potential in a large magmatic belt (Loucks, 2014; Richards, 2015).

The Gangdese belt, located in the southern Tibet, underwent the

processes of the Mesozoic subduction of Neo-Tethyan oceanic crust and the Cenozoic collision of Indian with Asian Blocks (Yin and Harrison, 2000; Chu et al., 2006; Hou et al., 2015a,b; Zhu et al., 2011, 2015, 2017). Collision-related porphyry Cu–Mo deposits are well developed in the Gangdese belt, forming a Cenozoic porphyry Cu–Mo deposit belt (Fig. 1; Hou et al., 2015a,b). In contrast, subduction-related porphyry Cu deposits are very rare with only one Jurassic porphyry Cu–Au deposit found so far, Xietongmen deposit (Tafti et al., 2014; Tang et al., 2015). This phenomenon is distinct from other subduction zones, such as the Andes belt, southwestern Pacific belt, and Central Asian Orogenic Belt, etc., which have belt-scale subduction-related porphyry Cu deposits (Sillitoe, 2010; Richards, 2015; Sun et al., 2015). The rarity of subduction-related (Jurassic) deposits are thought to be controlled by

* Corresponding author.

E-mail address: lianghy@gig.ac.cn (H. Liang).

<https://doi.org/10.1016/j.oregeorev.2019.103169>

Received 31 March 2019; Received in revised form 27 June 2019; Accepted 7 October 2019

Available online 11 October 2019

0169-1368/ © 2019 Elsevier B.V. All rights reserved.

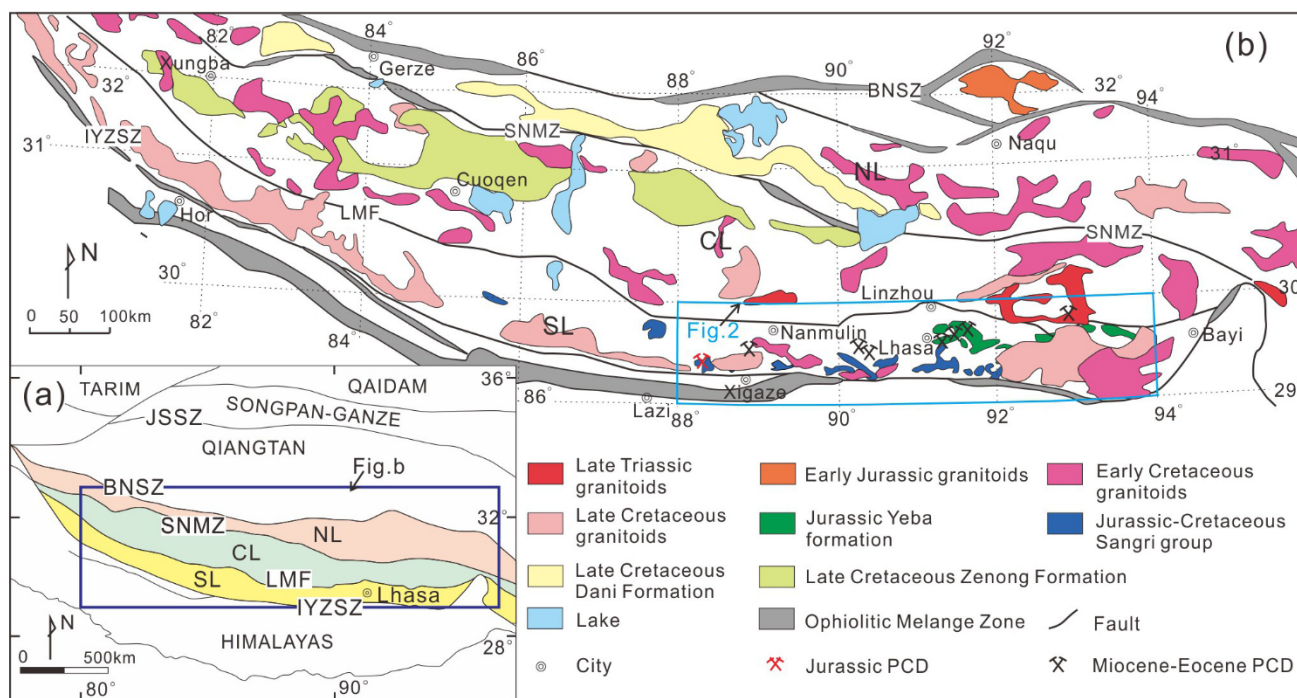


Fig. 1. (a) Tectonic framework of the Tibetan Plateau; (b) simplified geological map of the Lhasa terrane showing the distribution of igneous rocks (modified after Zhu et al., 2011). Abbreviations: JSSZ = Jinsha suture zone; BNSZ = Bangong–Nujiang suture zone; SNMZ = Shiquan River–Nam Tso Mélange Zone; LMF = Luobadui–Milashan Fault; IYZSZ = Indus–Yarlung Zangbo Suture Zone. SL = southern Lhasa subterrane, CL = central Lhasa subterrane, NL = northern Lhasa subterrane.

Jurassic magmatic fertility variations within the Gangdese belt (Hou et al., 2015b; Wang et al., 2017a) or late-stage erosion processes (Zou et al., 2017). However, no consensus has been reached on the variations in the fertility of Jurassic magmas, including the fertile western Gangdese belt (Hou et al., 2015b); fertile southern Gangdese belt (Wang et al., 2017a). Therefore, the spatial variations in the fertility of Jurassic arc magmas in the whole Gangdese belt need to be further constrained.

In this paper, we present mineral assemblage observations, whole-rock geochemistry, zircon U–Pb ages and trace element data from Jurassic magmatic rocks in the Gangdese belt. We combine these data with pre-existing published data to further explore the fertility of Jurassic magmas in the whole Gangdese belt.

2. Geological setting

The Lhasa terrane is one of the E–W trending terranes in the Tibetan Plateau, and is bounded by the Bangong–Nujiang suture zone (BNSZ) to the north and the Indus–Yarlung Zangbo suture zone (IYZSZ) to the south (Fig. 1; Yin and Harrison, 2000). The Lhasa terrane is divided into northern, central, and southern subterrane that are separated by the Shiquan River–Nam Tso Mélange Zone (SNMZ) and Luobadui–Milashan Fault (LMF) (Zhu et al., 2011). The central Lhasa subterrane has a Precambrian basement covered by widespread Carboniferous–Permian metasedimentary rocks and Late Jurassic–Early Cretaceous volcano-sedimentary sequences (Zhu et al., 2011, and references therein). Mesozoic granitoid rocks occur as widely distributed batholiths and stocks in the central Lhasa subterrane (Zhu et al., 2011; Cao et al., 2016). In contrast, the northern and southern Lhasa subterrane are underlain by juvenile Phanerozoic lower crust (Zhu et al., 2011; Hou et al., 2015a). The northern subterrane is overlain by Jurassic–Cretaceous sedimentary rocks and Lower Cretaceous volcano-sedimentary sequences, into which a Cretaceous granitoid batholith (~130 Ma to ~80 Ma) was intruded (Zhu et al., 2011; Hou et al., 2015a). Upper crustal rocks of the southern Lhasa subterrane are composed of Mesozoic and Paleogene–Eocene volcano-sedimentary sequences (including the Jurassic Yeba

Formation, Jurassic to Cretaceous Sangri Group, and Paleogene–Eocene Linzizong Group) and the Gangdese batholith (Zhu et al., 2011; Hou et al., 2015a).

The Gangdese batholith extends over 1500 km and is related to Mesozoic subduction of the Neo-Tethyan oceanic slab and the Cenozoic India–Asia continental collision. The batholith consists of sporadic small Late Triassic to Jurassic stocks and voluminous Cretaceous to Cenozoic intrusions (Fig. 2; Chu et al., 2006; Ji et al., 2009). The small Late Triassic to Jurassic stocks are calc-alkaline in composition, consisting chiefly of diorite, tonalite, granodiorite, monzogranite, and granite, with some gabbro and gabbroic diorite (Ji et al., 2009; Guo et al., 2013). The Cretaceous intrusions mainly comprise gabbro, diorite, granodiorite, monzogranite, tonalite, and some of them have adakite-like geochemical features (Wen et al., 2008a, b; Ji et al., 2009; Guan et al., 2010, 2011). The main lithologies of the Cenozoic intrusions include diorite, granodiorite, monzonite, monzogranite, and granite.

The main structures in the Gangdese belt include NE–SW, NW–SE, and N–S trending strike-slip faults, E–W trending thrust faults and shear zones. These structures formed in response to Miocene to Pliocene N–S compression and E–W extension (Fig. 2; e.g., Blisniuk et al., 2001; Coleman and Hodges, 1995).

3. Mineralization

The major period of porphyry copper mineralization in the Gangdese belt occurred as a consequence of post-collisional tectono-magmatic processes during the Oligocene–Miocene, and formed the Qulong, Jiama, Tinggong, Bangpu, Tangbula, and Zhunuo porphyry Cu–Mo deposits, etc. (e.g., Wang et al., 2014a,b; Hou et al., 2015a). However, only one Jurassic porphyry copper deposit formed in association with subduction, namely, Xietongmen (Xiongcu) porphyry Cu–Au deposit (Lang et al., 2014; Tafti et al., 2014; Tang et al., 2015). The Xietongmen (Xiongcu) porphyry Cu–Au deposit consists of two parts: (1) the Xietongmen deposit, which contains a resource of 219.8 Mt @ 0.43% Cu, 0.51 g/t Au and 3.87 g/t Ag, and (2) the Newtownmen

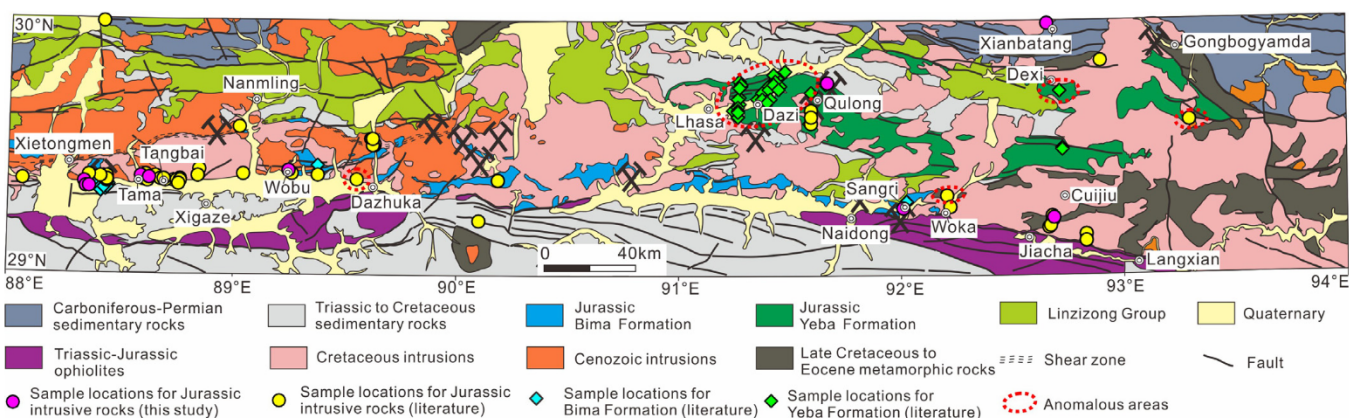


Fig. 2. Geological map of the Gangdese belt (modified after 1:200,000 geology maps, Guo et al., 2013; Zhang et al., 2014b). Sample locations (literature) are from Chen et al. (2009, 2011), Chen et al. (2019 and references therein), Chu et al. (2006), Dong and Zhang, 2013, Guo et al. (2013), Hou et al. (2015b), Huang et al. (2014a), Ji et al. (2009), Lang et al. (2014), Meng et al. (2016), Qu et al. (2007), Qiu et al. (2015), Shui et al. (2016, 2017), Tang et al. (2010), Tafti (2011), Wang et al. (2017a,b), Xu et al. (2017a,b), Xie et al. (2018a); Yang et al., 2011; Zhang et al. (2007), Zhu et al. (2011); Zou et al. (2015, 2017).

deposit, which hosts a resource of 388.9 Mt @ 0.32% Cu, 0.18 g/t Au and 0.87 g/t Ag. Ore-bearing porphyries for the Xietongmen deposit have zircon U-Pb ages of 172.9–162.4 Ma (Tafti et al., 2009; Lang et al., 2014), and the mineralization age for the Xietongmen deposit is 161.5 ± 2.7 Ma (molybdenite Re-Os dating, Lang et al., 2014). Ore-bearing porphyries for the Newtownmen deposit yield zircon U-Pb ages of 183.3–174.2 Ma (Tafti et al., 2009; Lang et al., 2014), and the mineralization age for the Newtownmen deposit is constrained by a molybdenite Re-Os age of 172.6 Ma (Lang et al., 2014).

4. Sampling

Twenty-six samples from eleven discrete Jurassic intrusions were collected from the Gangdese belt (Fig. 2). The petrography of these samples is listed in Table 1, and representative photographs are shown in Fig. 3. These samples mainly consist of quartz diorite, quartz diorite porphyry, granodiorite, and granodiorite porphyry that occur as small stocks or relics of varying size within the Cretaceous and Cenozoic granitic plutons.

5. Analytical methods

5.1. Whole-rock geochemistry

The least-altered samples were crushed by corundum plates and then powdered by an agate disk mill (< 200 mesh). The major and trace element analyses were performed at the State Key Laboratory of Isotope Geochemistry, Guangzhou Institute of Geochemistry, Chinese Academy of Sciences (SKLaBIG GIG CAS). Fused glass beads from the whole-rock powders were analyzed for major elements by a Rigaku ZSX100e X-ray fluorescence spectrometer with analytical uncertainties of 1 to 5 relative %. The detailed procedures are referred to in Goto and Tatsumi (1994) and Li et al. (2005). Trace element concentrations were analyzed by inductively coupled plasma mass spectrometry (ICP-MS), using a Perkin-Elmer ELAN 6000 instrument. Detailed procedures for sample dissolution, preparation and measurement are described by Li et al. (2002). Analytical accuracy and precision for trace elements analyses, estimated from measurements of USGS and Chinese national rock standards (BHVO-2, GSR-1, GSR-2, GSR-3, AGV-2, W-2, and SARM-4), were mostly better than 5 relative %. Major and trace element results are listed in Appendix 1.

5.2. Whole-rock Sr-Nd isotope

Whole rock Sr-Nd isotope analyses were conducted at the SKLaBIG

GIG CAS, using a Finnigan Neptune multi-collector ICP-MS. The sample rock powders were dissolved completely in a mixture of HF and HClO₄ at 120 °C for seven days. Detailed analytical procedures are described in Liang et al. (2003). Six unknown samples were analyzed after the NBS SRM 987 (Sr) and JNdi-1 (Nd) standards were analyzed. The measured Sr and Nd isotopic data were normalized to $^{86}\text{Sr}/^{88}\text{Sr} = 0.1194$ and $^{146}\text{Nd}/^{144}\text{Nd} = 0.7219$, respectively, to correct for mass fractionation. Measured standard materials yielded an average $^{87}\text{Sr}/^{86}\text{Sr}$ ratio of 0.710257 ± 0.000022 (1σ , $n = 4$) for NIST 987 and an average $^{143}\text{Nd}/^{144}\text{Nd}$ ratio of 0.512106 ± 0.000007 (1σ , $n = 4$) for Shin Etsu JNdi-1. The Sr-Nd isotope results are shown in Appendix 2.

5.3. Zircon U-Pb dating

All zircon grains were handpicked under a binocular microscope after separation from rock powders by heavy liquid and magnetic methods. These zircon grains were then mounted in an epoxy resin and polished to half of their respective thicknesses for analysis. Cathodoluminescence (CL) images, combined with transmitted and reflected light photomicrographs, were used to inspect the internal texture of the zircon grains. Suitable portions of each grain devoid of fracture and inclusions were chosen for analysis.

Zircon U-Pb dating and trace element analyses were conducted using an Agilent 7500a ICP-MS combined with a Resonetics RESOLUTION M-50 (193 nm ArF excimer) laser ablation system at GIG CAS. A constant laser energy of 80 mJ, a repetition rate of 8 Hz and a 31 μm spot size were used. The background acquisition time for each spot analysis was 30 s, followed by a data collection time of 40 s. The Temora zircon standard was used for the external calibration of the U-Pb dating (Black et al., 2003), while NIST SRM 610 was used as an external standard for the trace element analyses (Pearce et al., 1997). Detailed analytical procedures are referred to in Li et al. (2011). All obtained raw ICP-MS data was calculated using the ICPMSDataCal software (Liu et al., 2008). Zircon grains with < 90% concordance were excluded from the calculation of the final weighted mean $^{206}\text{Pb}/^{238}\text{U}$ age. The final weighted mean $^{206}\text{Pb}/^{238}\text{U}$ ages and Concordia diagrams were plotted using the Isoplot software (Ludwig, 2003). Errors for isotopic ratios on single analyses are reported at the 1σ level, and for weighted mean $^{206}\text{Pb}/^{238}\text{U}$ ages at the 2σ level. All of the results are shown in Appendix 3 and 4.

5.4. Zircon Hf isotope

Zircon Hf isotope analyses were undertaken at SKLaBIG GIG CAS using a Neptune Plus multi-collector ICP-MS equipped with a RESOLUTION M-50 (193 nm ArF excimer) laser ablation system. A 45 μm

Table 1
Sample information for the Jurassic granitoid rocks in the Gangdese belt: their locations, petrography, ages, and applied lithogeochemical and isotopic analyses.

Sample no.	Location	Longitude	Latitude	Lithology	Texture	Mineralogy and percentage (vol.%)	Age (Ma)	Age references	Zircon trace element	Zircon Hf isotope	major and trace elements	Sr-Nd isotope
XC-28-3	West of Xietongmen district	88.32	29.36	granodiorite	Equigranular	Pl (40–60%), Qtz (10–25%), Amp (5–15%), and Bi (5–10%) with accessory minerals of Zr, Ap, and Ttn	172.4 ± 1.2	this study	this study		this study	this study
XC-28-05	West of Xietongmen district	88.32	29.36	granodiorite	Equigranular						this study	
XC-40-4	West of Xietongmen district	88.33	29.34	granodiorite	Equigranular	Pl (45–55%), Qtz (10–15%), Amp (5–15%), Kfs (5–15%), and Bi (5–10%) with accessory minerals of Zr, Ap, and Ttn	171.6 ± 1.1	this study	this study	this study	this study	this study
XC-40-5	West of Xietongmen district	88.33	29.34	granodiorite	Equigranular						this study	
XC-79-01	West of Xietongmen district	88.34	29.34	quartz diorite porphyry	Porphyritic	Phenocrysts: Pl (10–25%), Qtz (5–15%), Amp (5–10%), and Bi (5–10%), in a matrix of Qtz, Pl, Amp, and Bi, with accessory minerals of Zr, Ap, and Ttn	178.9 ± 1.3	this study	this study		this study	
XC-79-02	West of Xietongmen district	88.34	29.34	quartz diorite porphyry	Porphyritic						this study	
XC-79-03	West of Xietongmen district	88.34	29.34	quartz diorite porphyry	Porphyritic						this study	
XC-15-2	Tama	88.58	29.38	granodiorite	Equigranular	Pl (40–55%), Qtz (25–35%), Amp (10–15%), Bi (5–10%), and accessory phases of Zr, Ap, and Ttn					this study	this study
XC-15-5	Tama	88.58	29.38	granodiorite	Equigranular						this study	this study
XC-15-6	Tama	88.58	29.38	granodiorite	Equigranular						this study	this study
14XC-33-02	Tangbai	88.62	29.38	granodiorite	Equigranular	Pl (40–50%), Qtz (25–35%), Amp (10–15%), and Bi (5–10%), and accessory phases of Zr, Ap, and Ttn	182.8 ± 1.6	this study	this study	this study	Guo et al., 2013	
14XC-36-02	Tangbai	88.65	29.36	granodiorite porphyry	Porphyritic	Phenocrysts: Pl (10–20%), Qtz (5–15%), Amp (5–10%), and Bi (5–10%), in a matrix of Qtz, Pl, Amp, and Bi, with accessory minerals of Zr, Ap, and Ttn	178.7 ± 1.3	this study	this study		Guo et al., 2013	
15XC-37-4	Wobu	89.25	29.40	quartz diorite porphyry	Porphyritic	Phenocrysts: Pl (15–20%), Amp (15–25%), in a matrix of Qtz, Pl, minor Kfs, and accessory Ap and Mt	166.3 ± 1.3	Zou et al., 2017	Zou et al., 2017	this study	this study	this study
15XC-37-5	Wobu	89.25	29.40	quartz diorite porphyry	Porphyritic						this study	this study
15XC-37-6	Wobu	89.25	29.40	quartz diorite porphyry	Porphyritic						this study	this study
15XC-37-8	Wobu	89.25	29.40	quartz diorite porphyry	Porphyritic						this study	this study
17XSR-1-3	Sangri	92.01	29.25	quartz diorite	Equigranular	Pl (40–45%), Amp (20–30%), Qtz (5–15%), and minor Bi (5–10%) with accessory minerals of Zr, Ap	184.5 ± 1.2	this study	this study		this study	
17XSR-1-4	Sangri	92.01	29.25	quartz diorite	Equigranular						this study	this study
17XCJ-9-1	Cuijiu	92.70	29.22	granodiorite	Equigranular	Pl (40–45%), Qtz (10–20%), Amp (10–15%), Bi (10–15%), and Kfs (5–10%), with accessory minerals of Zr, Ap, and Ttn	192.1 ± 1.3	this study	this study		this study	
17XCJ-9-5	Cuijiu	92.70	29.22	granodiorite	Equigranular						this study	this study
17XQL-1-1	Qulong district	91.67	29.74	granodiorite porphyry	Porphyritic	Phenocrysts: Pl (10–25%), Qtz (15–20%), and Amp (5–10%), in a matrix of Qtz, Pl, and Amp with accessory minerals of Zr, Ap	173.0 ± 1.1	this study	this study		this study	
17XQL-1-3	Qulong district	91.67	29.74	granodiorite porphyry	Porphyritic						this study	
17XXb-2-1	Xianbatang	92.66	30.00	quartz diorite	Equigranular	Pl (40–50%), Amp (15–20%), Qtz (10–20%), and Bi (5–15%) with accessory minerals of Zr, Ap	195.3 ± 1.3	this study	this study		this study	this study
17XXb-2-5	Xianbatang	92.66	30.00	quartz diorite	Equigranular						this study	this study
17XXb-2-2	Xianbatang	92.66	30.00	quartz diorite	Equigranular						this study	this study
17XXb-2-4	Xianbatang	92.66	30.00	quartz diorite	Equigranular						this study	this study

Amp = amphibole, Bi = biotite, Kfs = K-feldspar, Mt = magnetite, Pl = plagioclase, Qtz = quartz, Ttn = titanite.

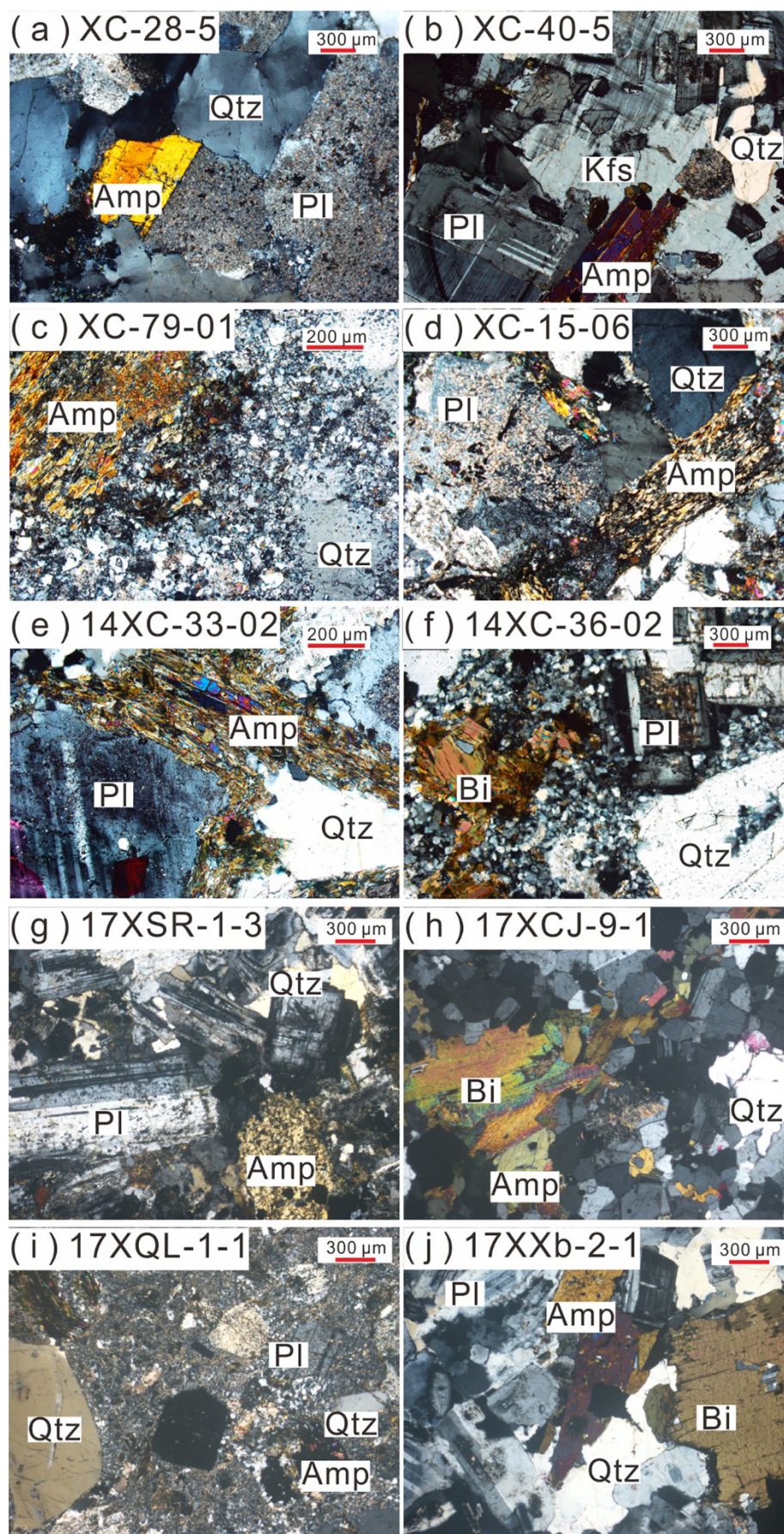


Fig. 3. Photomicrographs of Jurassic granitoid rocks. Amp = Amphibole; Bi = biotite; Pl = plagioclase; Qtz = quartz.

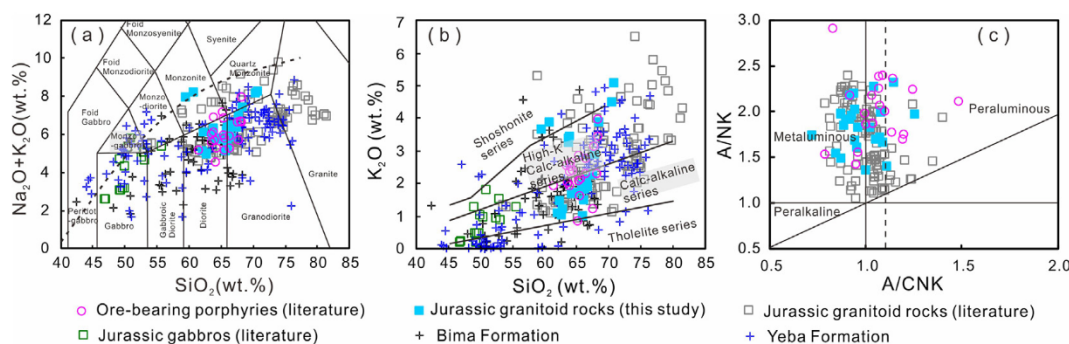


Fig. 4. (a) Total alkali vs. SiO_2 (TAS) diagram (after Le Maitre et al. (1989)); (b) K_2O vs. SiO_2 diagram (after Rickwood, 1989). (c) A/NK vs. A/CNK diagram (after Maniar and Piccoli, 1989) for the Jurassic granitoid rocks, gabbroic rocks, and Xietongmen ore-bearing porphyries. Data for the Jurassic granitoid rocks, gabbroic rocks, and volcanic rocks are from this study, Chen et al. (2011), Chen et al. (2019 and references therein), Chu et al. (2006), Dong and Zhang (2013), Guo et al. (2013), Hou et al. (2015b), Huang et al. (2014a), Meng et al. (2016), Qu et al. (2007), Qiu et al. (2015), Shui et al. (2016, 2017), Tang et al. (2010), Tafti (2011), Wang et al. (2017b), Xie et al. (2018a), Xu et al. (2017a,b), Yang et al. (2011), Zhang et al. (2007), Zhu et al. (2011), Zou et al. (2015, 2017). Data for the Xietongmen ore-bearing porphyries are from Huang et al. (2011), Qu et al. (2007), Tafti (2011), and Yin et al. (2017).

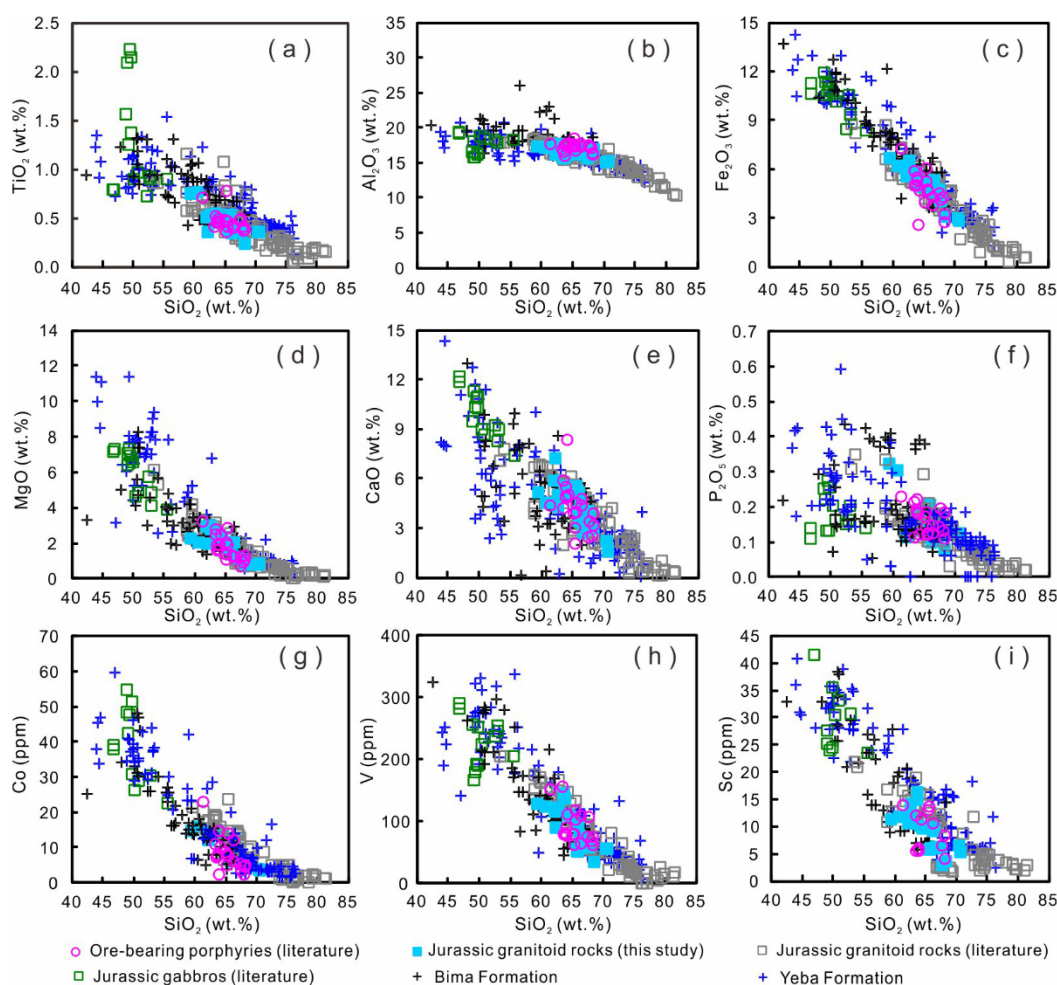


Fig. 5. Harker diagrams of the Jurassic granitoid rocks, gabbroic rocks, and Xietongmen ore-bearing porphyries. The whole-rock major element compositions are recalculated to 100% on a volatile-free basis. Data sources are the same as for Fig. 4.

laser beam size and a laser repetition rate of 10 Hz were adopted during the analysis. Details of the instrument conditions and data acquisition were similar to those in Wu et al. (2006) and Zhang et al. (2014a). Two Penglai standard zircons (Li et al., 2010) were analyzed before every six zircon samples. Detailed data reduction procedures are reported in Zhang et al. (2015). The $\varepsilon_{\text{Hf}}(t)$ values were calculated using a ^{176}Lu decay constant of $1.867 \times 10^{-11} \text{ a}^{-1}$ (Soderlund et al., 2004), and chondritic $^{176}\text{Hf}/^{177}\text{Hf}$ values of 0.0332 and $^{176}\text{Lu}/^{177}\text{Hf}$ of 0.282772

(Blichert-Toft and Albarede, 1997). The two-stage model age ($T_{2\text{DM}}$) were calculated in reference to the present-day $^{176}\text{Hf}/^{177}\text{Hf}$ ratio (0.28325), the depleted mantle $^{176}\text{Lu}/^{177}\text{Hf}$ ratio (0.0384) (Griffin et al., 2000), and a mean $^{176}\text{Lu}/^{177}\text{Hf}$ ratio of 0.015 for the average continental crust (Griffin et al., 2002). The Hf isotopic data are listed in Appendix 5.

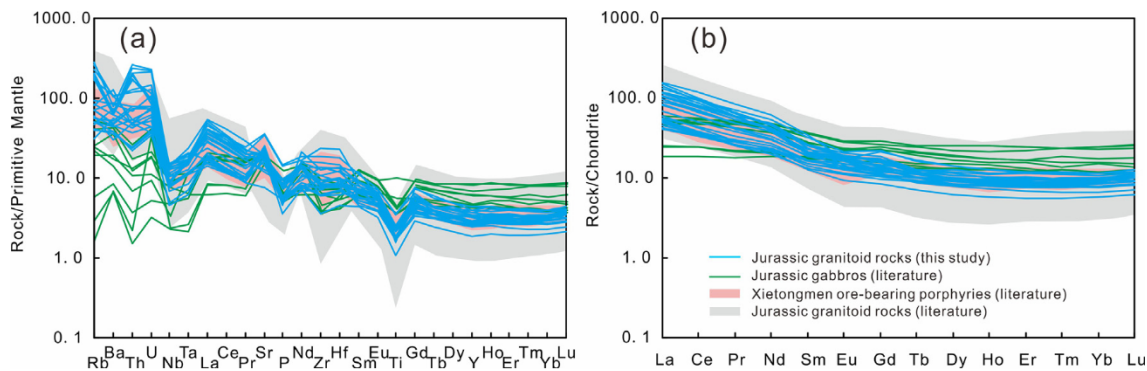


Fig. 6. (a) Primitive mantle-normalized trace element diagrams and (b) Chondrite-normalized REE patterns for the Jurassic granitoid rocks, gabbroic rocks, and Xietongmen ore-bearing porphyries. Normalization values for primitive mantle and chondrite are from Sun and McDonough (1989). Data sources are the same as for Fig. 4.

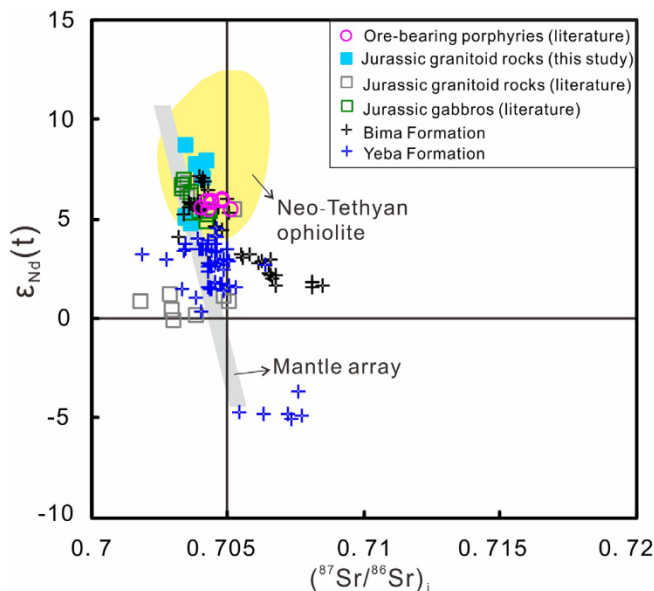


Fig. 7. $(^{87}\text{Sr}/^{86}\text{Sr})_i$ vs. $\epsilon_{\text{Nd}}(t)$ diagram for the Jurassic granitoid rocks, gabbroic rocks, and Xietongmen ore-bearing porphyries. Data sources for the Jurassic granitoid rocks, gabbroic rocks, and volcanic rocks are from this study, (Chen et al., 2019 and references therein), Chu et al. (2006), Hou et al., 2015b, Tafti (2011), Wang et al. (2017b), Xu et al. (2017a,b), Yang et al., 2011. Data for the Xietongmen porphyries are from Qu et al. (2007), Yin et al., 2017, Tafti (2011). Data for the Neo-Tethyan ophiolites are from Mahoney et al., 1998; Xu and Castillo, 2004; Zhang et al., 2005.

6. Results

6.1. Whole-rock geochemistry results

Whole-rock geochemical data for the granitoid samples from this study are listed in Appendix 1. Most samples are fresh and only several samples have been slightly altered by potassic alteration, chloritization, epidotization, and/or sericitization, and this may be reflected by some scatter in their alkali contents and large-ion lithophile element compositions.

Major elements: All granitoid samples collected for this study have SiO_2 contents of 59.4 to 70.7 wt%, $\text{K}_2\text{O} + \text{Na}_2\text{O}$ contents of 4.96 to 8.31 wt%, and Mg# values of 35 to 53 (normalized to 100% volatile free). They mostly plot in the diorite and granodiorite fields on the TAS diagram, with several samples falling in the monzonite and quartz monzonite fields (Fig. 4a). These granitoids mainly plot in the calc-alkaline and high-K calc-alkaline series fields on the K_2O versus SiO_2 diagram (Fig. 4b), with some samples falling into the shoshonite series

field, potentially as a consequence of potassic alteration. They are metaluminous to peraluminous with A/CNK values of 0.72–1.25 (mainly < 1.1; Fig. 4c). Published data for Jurassic granitoid rocks (including the Xietongmen ore-bearing porphyries) in the Gangdese belt indicate that they have a wider range of SiO_2 contents (58.9 to 81.4 wt%), and they plot in the diorite, granodiorite and granite fields on the TAS diagram, with minor plotting in the monzodiorite, monzonite and quartz monzonite fields (Fig. 4a). They mainly fall into the calc-alkaline and high-K calc-alkaline series on the K_2O versus SiO_2 diagram, with some samples falling into the shoshonite series field, which may be due to potassic alteration (Fig. 4b). They have A/CNK values of 0.78–1.67 (mainly < 1.1, Fig. 4c), which overlaps with our data. All of the granitoid rocks from both this study and the pre-existing literature show that most major oxides and some trace elements correlate with SiO_2 and have linear compositional trends in Harker diagrams (Fig. 5).

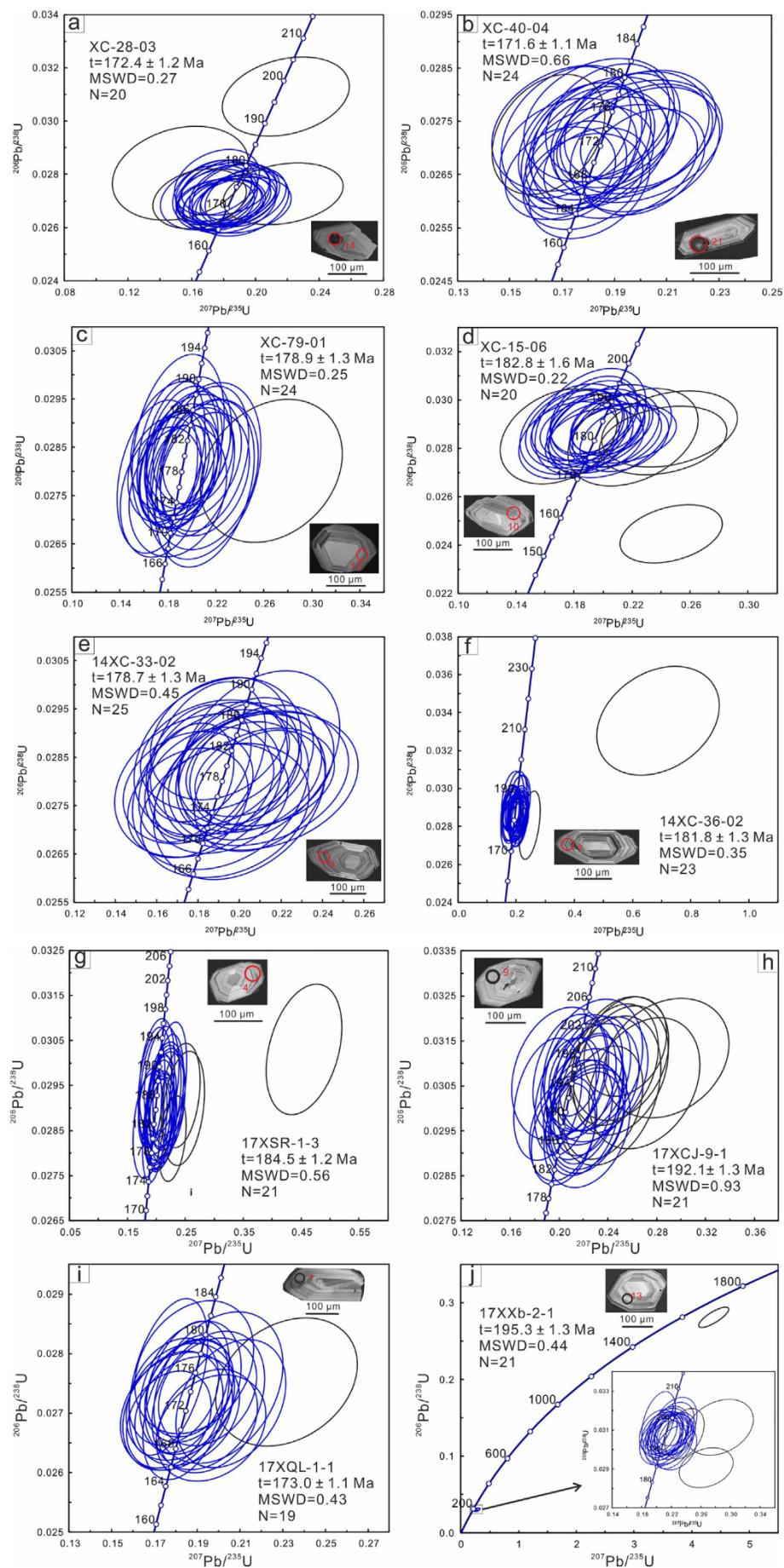
Trace elements: Primitive mantle-normalized trace element diagrams and chondrite-normalized rare earth element (REE) patterns are similar across all samples and show features typical of subduction-related magmas (Pearce and Peate, 1995). The granitoid rocks from this study are characterized by enrichment in large-ion lithophile elements (LILE; e.g., Ba, Th, U), and depletion in high field strength elements (HFSE; e.g., Nb, Ta, Ti) (Fig. 6a). They are enriched in LREE ((La/Yb)_N = 5.13–15.02) (Fig. 6b) and they have weakly negative to positive Eu anomalies, with $\text{Eu}_N/\text{Eu}_N^*$ values of 0.62–1.03 (where $\text{Eu}_N/\text{Eu}_N^* = 2 \times \text{Eu}_N/(\text{Sm}_N + \text{Gd}_N)$). Our data are similar to the other published data for Jurassic granitoid rocks (including the Xietongmen ore-bearing porphyries) in the Gangdese belt on the primitive mantle-normalized trace element and chondrite-normalized rare earth element (REE) diagrams (Fig. 6a, b).

6.2. Sr-Nd isotopic results

All of the granitoid rocks from this study have depleted Sr-Nd isotopic compositions, with $(^{87}\text{Sr}/^{86}\text{Sr})_i$ ratios of 0.703414–0.704085, and $\epsilon_{\text{Nd}}(t)$ values of 4.8–8.7 (Appendix 2; Fig. 7). Two-stage Nd model ages ($T_{\text{DM}2}$) range from 255 to 562 Ma. Published data for the Jurassic granitoid rocks in the Gangdese belt have a wider range of Sr-Nd isotopic compositions ($(^{87}\text{Sr}/^{86}\text{Sr})_i$ = 0.701752 to 0.705203; $\epsilon_{\text{Nd}}(t)$ = −0.1 to 6.8, mainly > 3).

6.3. Zircon U-Pb ages

Zircon grains from all of the granitoid rocks in this study are euhedral and have lengths of 100 μm to 150 μm with length/width ratios of 1:2–1:3. All zircon grains exhibit oscillatory zoning in CL images and have Th/U ratios of 0.14–1.43, indicative of a magmatic origin. Zircon U-Pb dating results are shown in Appendix 3.



(caption on next page)

Fig. 8. Zircon U-Pb Concordia diagrams and CL images of representative zircon grains from the Jurassic granitoid rocks. The grey circles are the spots precluded from the final weighted mean $^{206}\text{Pb}/^{238}\text{U}$ age calculations.

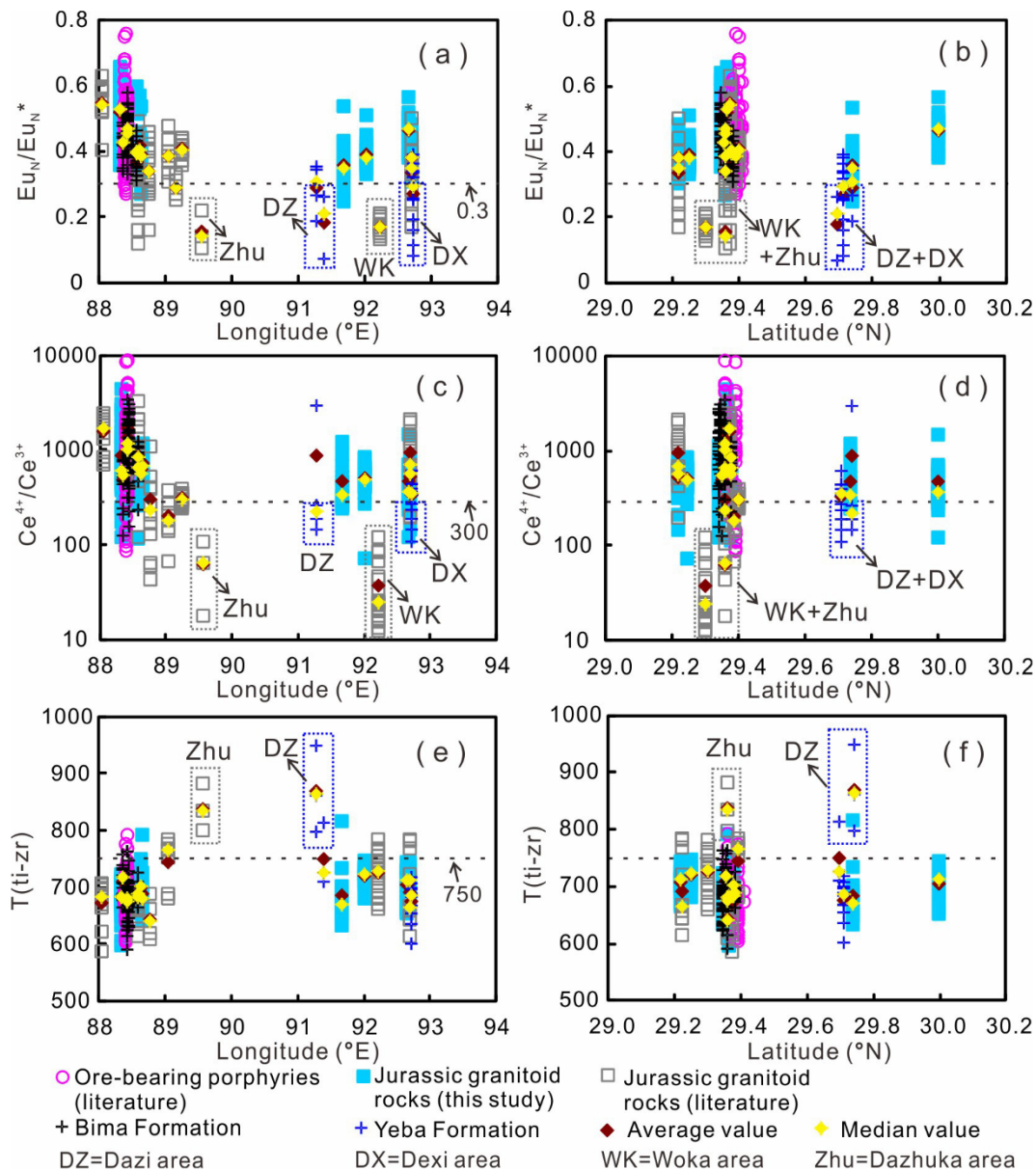


Fig. 9. Along-arc and across-arc variations in zircon trace element ratios and titanium-in-zircon temperatures from the Jurassic magmatic rocks ($\text{SiO}_2 = 58\text{--}70\text{ wt}\%$): (a) $\text{Eu}_\text{N}/\text{Eu}_\text{N}^*$ vs. Longitude; (b) $\text{Eu}_\text{N}/\text{Eu}_\text{N}^*$ vs. Latitude; (c) $\text{Ce}^{4+}/\text{Ce}^{3+}$ vs. Longitude; (d) $\text{Ce}^{4+}/\text{Ce}^{3+}$ vs. Latitude; (e) Tt-zr ($^\circ\text{C}$) vs. Longitude; (f) Tt-zr ($^\circ\text{C}$) vs. Latitude. Data sources for Jurassic magmatic rocks are from this study, Chen et al. (2019) and references therein, Wang et al. (2017a), Xie et al. (2018a). Data for the Xietongmen porphyries are from this study, Xie et al. (2018b), Wang et al. (2017a), and Zou et al. (2015).

Zircon grains with $< 90\%$ concordance and inherited and/or xenocryst zircons were omitted before calculation of the average weighted mean ages. Granodiorite samples (XC-28-03 and XC-40-04) in the west Xietongmen district have a weighted mean age of $172.4 \pm 1.2\text{ Ma}$, with $\text{MSWD} = 0.27$ (Fig. 8a), and $171.6 \pm 1.1\text{ Ma}$, with $\text{MSWD} = 0.66$ (Fig. 8b), respectively. Quartz diorite porphyry sample XC-79-01 in the west Xietongmen district has a weighted mean age of $178.9 \pm 1.3\text{ Ma}$, with $\text{MSWD} = 0.25$ (Fig. 8c). A granodiorite sample (XC-15-06) from the Tama area yielded a final weighted mean age of $182.8 \pm 1.6\text{ Ma}$, with $\text{MSWD} = 0.22$ (Fig. 8d). A granodiorite sample (14XC-33-02) and granodiorite porphyry sample (14XC-36-02) from the Tangbai area have a weighted mean age of $178.7 \pm 1.3\text{ Ma}$, with $\text{MSWD} = 0.45$ (Fig. 8e), and $181.8 \pm 1.3\text{ Ma}$, with $\text{MSWD} = 0.35$

(Fig. 8f), respectively. A quartz diorite sample (17XSR-1-3) from the Sangri area yielded a weighted mean age of $184.5 \pm 1.2\text{ Ma}$, with $\text{MSWD} = 0.56$ (Fig. 8g). A granodiorite sample (17XCJ-9-1) from the Cuijiu area yielded a weighted mean age of $192.1 \pm 1.3\text{ Ma}$, with $\text{MSWD} = 0.93$ (Fig. 8h). A granodiorite porphyry sample (17XQL-1-1) from the Qulong district has a weighted mean age of $173.0 \pm 1.1\text{ Ma}$, with $\text{MSWD} = 0.43$ (Fig. 8i). A quartz diorite sample (17XXb-2-1) from the Xianbatang area yielded a weighted mean age of $195.3 \pm 1.3\text{ Ma}$, with $\text{MSWD} = 0.44$ (Fig. 8j).

6.4. Zircon trace element results and titanium-in-zircon temperatures

Zircon trace element results are easily contaminated by mineral

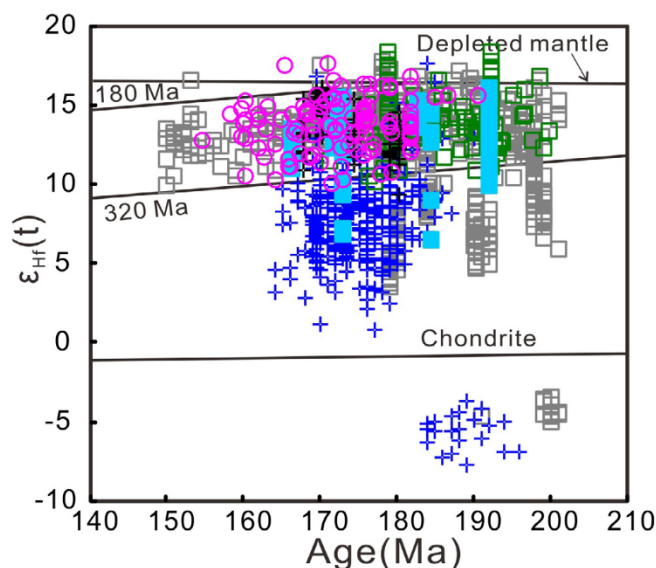


Fig. 10. Zircon U-Pb age vs. $\epsilon_{\text{Hf}}(t)$ values for the Jurassic granitoid rocks, gabbroic rocks, and Xietongmen ore-bearing porphyries. Data for the Jurassic granitoid rocks, gabbroic rocks, and volcanic rocks are from this study, Chen et al. (2019 and references therein), Ma et al. (2017a,b), Chu et al. (2006), Ji et al. (2009), Meng et al. (2016), Qiu et al. (2015), Wang et al. (2017a,b), Xu et al. (2017b), Dong and Zhang (2013), Shui et al. (2017), Zhang et al. (2007), Zhu et al. (2011); Xie et al. (2018a,b). Data for the Xietongmen ore-bearing porphyries are from Hou et al. (2015b), Huang et al. (2014a,b), Tang et al. (2015), and Yin et al. (2017).

inclusions in zircon during LA-ICP-MS analysis. Therefore, zircon trace element data with La > 0.1 ppm and Ti > 50 ppm are excluded, to avoid contamination by other REE-bearing minerals and Ti-(Fe) oxides. Xenocrystic zircon grains or grains with low concordance (< 90%) were also filtered out. The final zircon trace element results are listed in Appendix 4, and zircon rare earth element patterns are presented in Appendix Fig. 1. The zircon grains from the granitoid rocks from this study are characterized by positive Ce anomalies, and are depleted in LREE and enriched in HREE. Jurassic granitoid rocks from this study have high average zircon $\text{Eu}_\text{N}/\text{Eu}_\text{N}^*$ (> 0.3), and $\text{Ce}^{4+}/\text{Ce}^{3+}$ (> 300) ratios. This is similar to those of most published Jurassic magmatic rocks, except for the granitoid rocks in the Dazhuka (Zhu) and Woka (WK) areas and the Yeba Formation in the Dazi and Dexi areas (DZ and DX; Fig. 9a–d).

Considering these Jurassic granitoid rocks are silica-oversaturated and contain titanite (this study; Guo et al., 2013; Xie et al., 2018a), parameters of $a\text{SiO}_2 = 1$ and $a\text{TiO}_2 = 0.7$ were adopted to calculate the T(ti-zr) values (Ferry and Watson, 2007; McDowell et al., 2014). The estimated temperatures show low average T(ti-zr) values of < 750 °C for the Jurassic granitoid rocks from this study, similar to those calculated for published Jurassic magmatic rocks in the Gangdese belt, except the granitoid rocks in the Dazhuka area (Zhu) and Yeba Formation (DZ; Fig. 9e, f).

6.5. Zircon Hf isotopic results

All the granitoid rocks analyzed from this study have similar zircon Hf isotopic compositions (Appendix 5; Fig. 10). They all have positive $\epsilon_{\text{Hf}}(t)$ values ranging from 6.5 to 16.0, with corresponding two-stage model ages ($T_{\text{DM}2}$) of 206 Ma to 810 Ma. Jurassic magmatic rocks in the whole Gangdese belt from the literature have a wider range of Hf isotope compositions ($\epsilon_{\text{Hf}}(t) = -5.0$ to 17.7; mainly in 5–17) (Fig. 10).

7. Discussion

7.1. Ages

Our new data for 10 granitoid rocks in the Gangdese belt show zircon U-Pb ages ranging from 195.3 ± 1.3 Ma to 171.6 ± 1.1 Ma. These ages are similar to those published ages of Jurassic granitoid rocks in the whole Gangdese belt (with zircon U-Pb ages of 201.3–149.1 Ma, peaking at 185–170 Ma; Chu et al., 2006; Tafti, 2011; Guo et al., 2013; Qiu et al., 2015; Meng et al., 2016; Wang et al., 2017b; Xu et al., 2017a; Zou et al., 2017; Xie et al., 2018a). The published data on the ore-bearing quartz diorite porphyries have zircon U-Pb ages of 172.9–162.4 Ma for the Xietongmen deposit and 183.3–174.2 Ma for the Newtongmen deposit (Tafti et al., 2009; Lang et al., 2014). Taken together, a period of magmatism developed in the Gangdese belt that was coeval with the Xietongmen porphyry copper mineralization. Moreover, all of these granitoid rocks have ages that overlap with those of the Yeba and Bima volcanic rocks (195–174 Ma; Zhu et al., 2008; Kang et al., 2014; Chen et al., 2019 and references therein) in the Gangdese belt, which are predominantly regarded as products of northward-subduction of Neo-Tethyan oceanic crust (e.g., Kang et al., 2014; Ma et al., 2017a, b; Liu et al., 2018).

7.2. Petrogenesis

The Jurassic granitoid rocks in the Gangdese belt are mainly calc-alkaline to high-K calc-alkaline in composition. They show enrichment in LREE and LILEs, and depletion in HREE and HFSEs, which are typical of arc-related magmatic rocks (Fig. 6, Pearce and Peate, 1995; Hawkesworth et al., 1997). Intermediate to felsic arc-related magmas are usually thought to be generated through the MASH process (melting, assimilation, storage, and homogenization; Hildreth and Moorbath, 1988) or “hot zones” (Annen et al., 2006). These magmas are widely accepted to be formed by interaction between hot, hydrous, mantle-wedge-derived basaltic magmas and lower crustal lithologies. The Jurassic granitoid rocks are typical of arc-related magmatic rocks, which could be generated by the MASH process. During the MASH process, crystal fractionation occurs at different crustal depths (Annen et al., 2006). The Jurassic granitoid rocks show decreasing trends of TiO_2 , Al_2O_3 , Fe_2O_3 , MgO , CaO , P_2O_5 with increasing of SiO_2 (Fig. 5), which suggest that they underwent fractionations of pyroxene, amphibole, Fe-Ti oxides and apatite. They have negative relationships between Co, V, Sc and SiO_2 (Fig. 5), consistent with the fractionation of pyroxene. The occurrence of amphibole as a phenocryst in the porphyries, together with listric chondrite-normalized REE patterns of the Jurassic granitoid rocks indicate the early fractionation of amphibole (Fig. 6a, b). The increasing of Na_2O , K_2O with increasing of SiO_2 (not shown) may support the late fractionation of plagioclase and K-feldspar. All of the evidences above suggest that the Jurassic granitoid rocks underwent crystal fractionation during the MASH process.

As the southern Lhasa subterrane is characterized by juvenile lower crust, the juvenile lower crust has isotopic features similar to those of the depleted sub-arc mantle (Zhu et al., 2011). Therefore, interaction between the mantle-derived basaltic magmas and the juvenile lower crust will not change the general depleted Sr-Nd-Hf isotopic features of the magmas parental to the Jurassic granitoid rocks in the Gangdese belt (Figs. 7 and 10). Some scattered Sr-Nd-Hf compositions in Jurassic granitoid rocks in the Gangdese belt indicate that variably evolved crustal components were locally involved (Zhu et al., 2011; Chen et al., 2019; Figs. 7 and 10).

7.3. Geochemical variations and the magma fertility of Jurassic magmatic rocks in the Gangdese belt

Ore-bearing intrusions of porphyry copper deposits worldwide commonly have SiO_2 contents of 58–70 wt% (Loucks, 2014). Jurassic

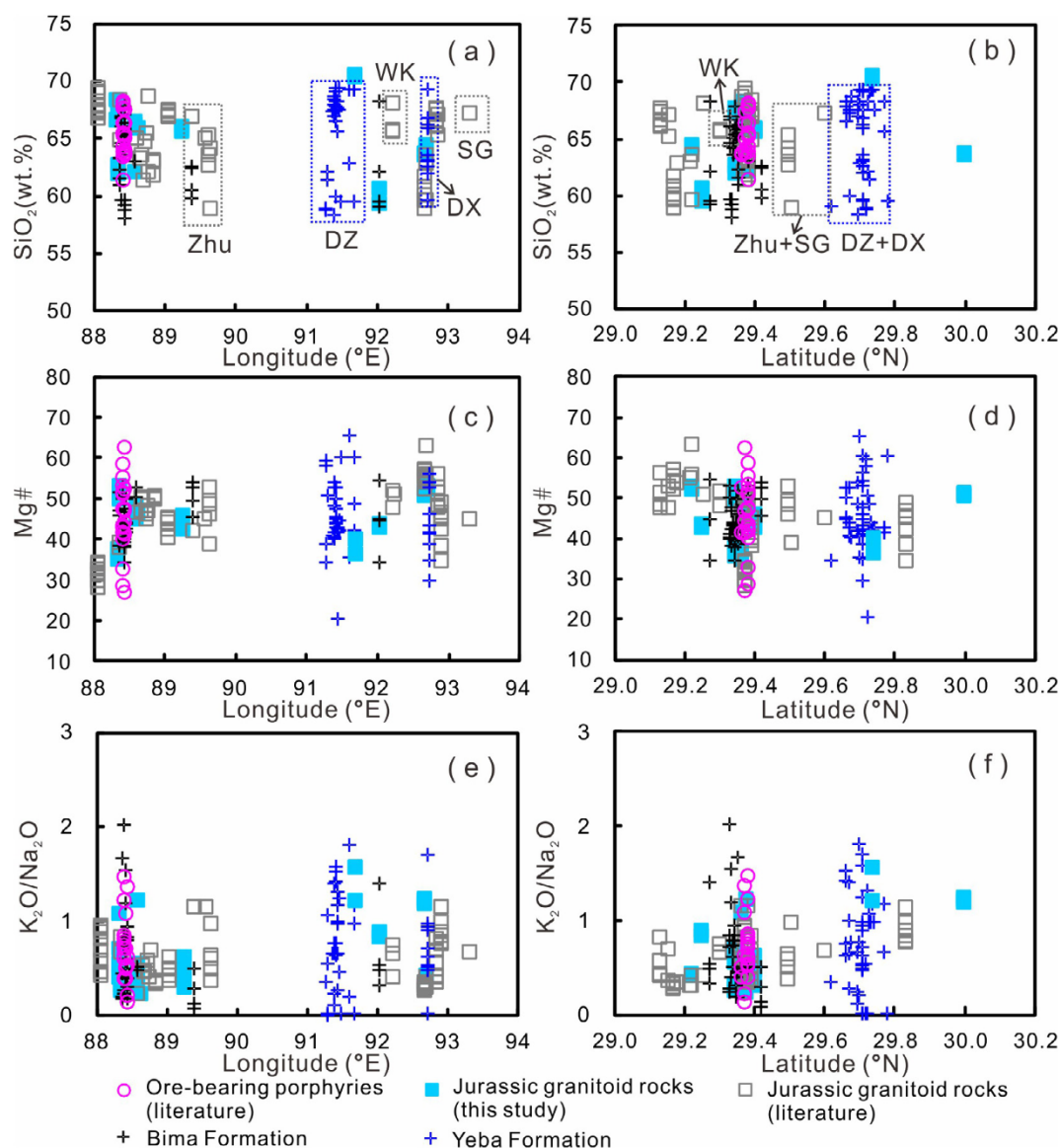


Fig. 11. Along-arc and across-arc geochemical variations of the Jurassic magmatic rocks ($\text{SiO}_2 = 58\text{--}70\text{ wt\%}$): (a) SiO_2 vs. Longitude; (b) SiO_2 vs. Latitude; (c) Mg# vs. Longitude; (d) Mg# vs. Latitude; (e) $\text{K}_2\text{O}/\text{Na}_2\text{O}$ vs. Longitude; (f) $\text{K}_2\text{O}/\text{Na}_2\text{O}$ vs. Latitude. Data sources are the same as for Fig. 4.

magmatic rocks with SiO_2 contents of 58–70 wt% (including granitoid rocks and volcanic rocks with ages of 150–201 Ma) were used to evaluate their geochemical variability and their fertility for the subduction-related porphyry copper deposits in the Gangdese belt.

The compositions of Jurassic magmatic rocks (with $\text{SiO}_2 = 58\text{--}70\text{ wt\%}$) from the Gangdese belt both in this study and the published literature do not demonstrate systematic along-arc ($88^\circ\text{E}\text{--}94^\circ\text{E}$) or across-arc ($29^\circ\text{N}\text{--}30^\circ\text{N}$) geochemical variations. The SiO_2 contents, Mg# values, and $\text{K}_2\text{O}/\text{Na}_2\text{O}$ ratios of the Jurassic magmatic rocks show similar ranges and are constant along-arc and across-arc in the Gangdese belt (Fig. 11). Similarly, the Jurassic magmatic rocks do not show apparent along-arc or across-arc Sr–Nd–Hf isotopic variations in the Gangdese belt, instead, they show generally depleted Sr–Nd–Hf isotopic compositions in the whole belt (Fig. 12a–d). Locally, some Jurassic magmatic rocks have more enriched Sr–Nd–Hf isotopic characteristics in the Bima Formation of the south of Xietongmen district (SX), the granitoid rocks in the Woka area (WK), ~30 km south of the Gongbogyamda area (SG) and the occurrences of the Yeba Formation (Fig. 12e, f). These geochemical characteristics indicate that the Jurassic magmatic rocks were generally derived from a similar depleted mantle source, with some evolved crustal components involved in the

some localized areas.

Hydrous and oxidized magmas are usually fertile for porphyry Cu deposit (Richards, 2003; Liang et al., 2009; Sillitoe, 2010; Sun et al., 2013; Huang et al., 2013, 2018). The occurrence of amphibole, relatively high whole-rock $\text{Al}_2\text{O}_3/\text{TiO}_2$ and Sr/Y ratios, and a low titanium-in-zircon temperature directly or indirectly reflect high water contents in arc magmas (Loucks, 2014; Richards, 2015; Wang et al., 2017a). Amphiboles commonly occur in the Jurassic magmatic rocks in the whole Gangdese belt, based on a survey of the extensive literature on the petrology of Jurassic magmatic rocks within this belt and our samples. Most of the Jurassic magmatic rocks, either along-arc or across-arc, in the Gangdese belt have whole-rock $\text{Al}_2\text{O}_3/\text{TiO}_2 > 15$ and Sr/Y ratios > 20 (Fig. 13a–d), similar to those of the ore-bearing intrusions worldwide (Loucks, 2014), and most of them have low average titanium-in-zircon temperatures of 640–733 °C. Some low Sr/Y ratios and high average titanium-in-zircon temperatures ($> 750^\circ\text{C}$) locally occur (Figs. 2, 9e, f, 13c, d).

On the other hand, mineral assemblages, whole rock V/Sc ratios and zircon $\text{Eu}_\text{N}/\text{Eu}_\text{N}^*$ and $\text{Ce}^{4+}/\text{Ce}^{3+}$ ratios are commonly used as indicators for magma oxidation state (Ballard et al., 2002; Liang et al., 2006; Loucks, 2014; Dilles et al., 2015). Many of the Jurassic granitic

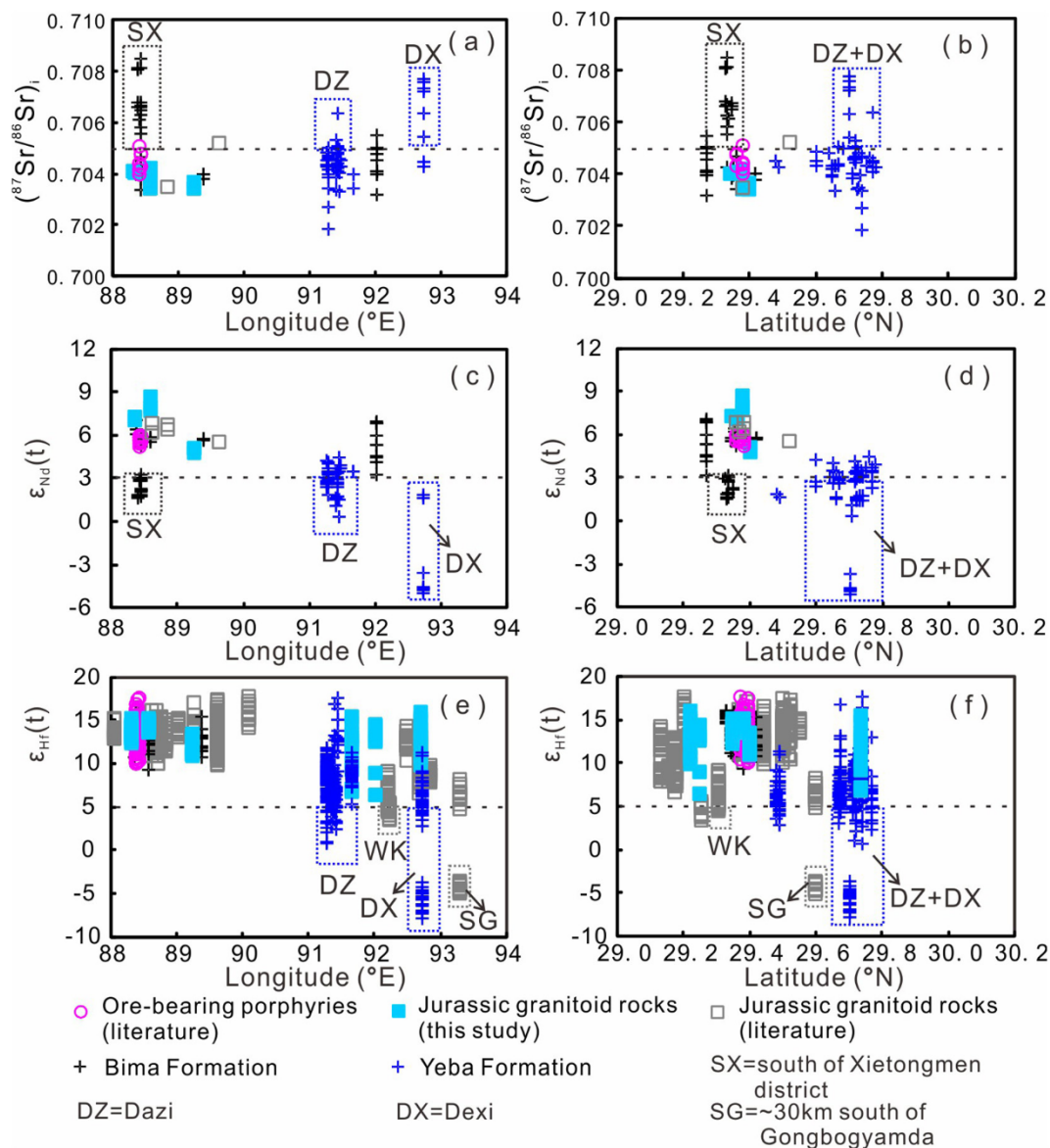


Fig. 12. Along-arc and across-arc Sr-Nd-Hf isotopic variations of the Jurassic magmatic rocks: (a) $^{87}\text{Sr}/^{86}\text{Sr}_i$ vs. Longitude; (b) $^{87}\text{Sr}/^{86}\text{Sr}_i$ vs. Latitude; (c) $\epsilon_{\text{Nd}}(t)$ vs. Longitude; (d) $\epsilon_{\text{Nd}}(t)$ vs. Latitude; (e) $\epsilon_{\text{Hf}}(t)$ vs. Longitude; (f) $\epsilon_{\text{Hf}}(t)$ vs. Latitude. Data sources are the same as for Figs. 7 and 10.

rocks in the Gangdese belt have a mineral assemblage of titanite + magnetite + quartz, such as the granodiorites in the west of the Xietongmen district, in the Tama area, in the Tangbai area and the Cuijiu area, and the quartz diorite porphyry in the Wobu area (Zou et al., 2017 and this study), which indicate that they crystallized from oxidized magmas (Wones, 1989; Harlov et al., 2006). The Jurassic magmatic rocks in the Gangdese belt generally have whole-rock V/Sc (> 8) ratios (Fig. 13e, f) close to the values from intrusions related to the giant porphyry Cu-Au deposits (whole-rock V/Sc > 10, Loucks, 2014). Furthermore, fertile magmatic suites have collectively higher zircon $\text{Eu}_N/\text{Eu}_N^*$ (> 0.3) and $\text{Ce}^{4+}/\text{Ce}^{3+}$ (> 300 in Chile; > 120 in Yulong belt, Tibet) ratios than barren magmatic suites (Ballard et al., 2002; Liang et al., 2006; Lu et al., 2016). Most of the Jurassic magmatic rocks in the Gangdese belt have high average zircon $\text{Eu}_N/\text{Eu}_N^*$ (> 0.3) and average zircon $\text{Ce}^{4+}/\text{Ce}^{3+}$ (> 300) ratios. Some Jurassic magmatic rocks with low whole-rock V/Sc ratios and zircon $\text{Eu}_N/\text{Eu}_N^*$, $\text{Ce}^{4+}/\text{Ce}^{3+}$ ratios occur in localized areas, such as the granitoid rocks in Dazhuka (Zhu), Woka (WK), and ~30 km south of the Gongbogyamda area (SG) and the Yeba Formation (DZ and DX; Figs. 2, 9a–d, 13e, f). The above characteristics suggest that the Jurassic arc magmas

generated in the Gangdese belt were generally water-rich and oxidized, except for some anomalous localized areas with a low magmatic water content and oxidation state. The water-rich and oxidized nature of the Jurassic arc magmas were fertile for the porphyry Cu mineralization.

Some of the Jurassic magmatic rocks that are restricted to the anomalous localized areas have low magmatic water contents and low oxidation states. These localized magmatic rocks have nearly overlapping SiO_2 contents, follow the same evolutionary trends in Harker diagrams as and share similar trace element and REE patterns with the water-rich and oxidized magmas (Figs. 5, 6, 11a, b), which indicate that they experienced a similar degree of magma fractionation. Moreover, the Gangdese crust was reported as generally having a normal thickness from 200 Ma to ~70 Ma (~37 km; Zhu et al., 2017). The above characteristics suggest that magma fractionation and crustal thickness could not play an important role in the genesis of the localized anomalies. The Jurassic magmatic rocks from the anomalous areas show more enriched Sr-Nd-Hf isotope than rocks that crystallized from water-rich and oxidized magmas (Fig. 12), which suggest that crustal contamination was involved in their generation. Therefore, crustal contamination was likely to be the main cause of their anomalous geochemical

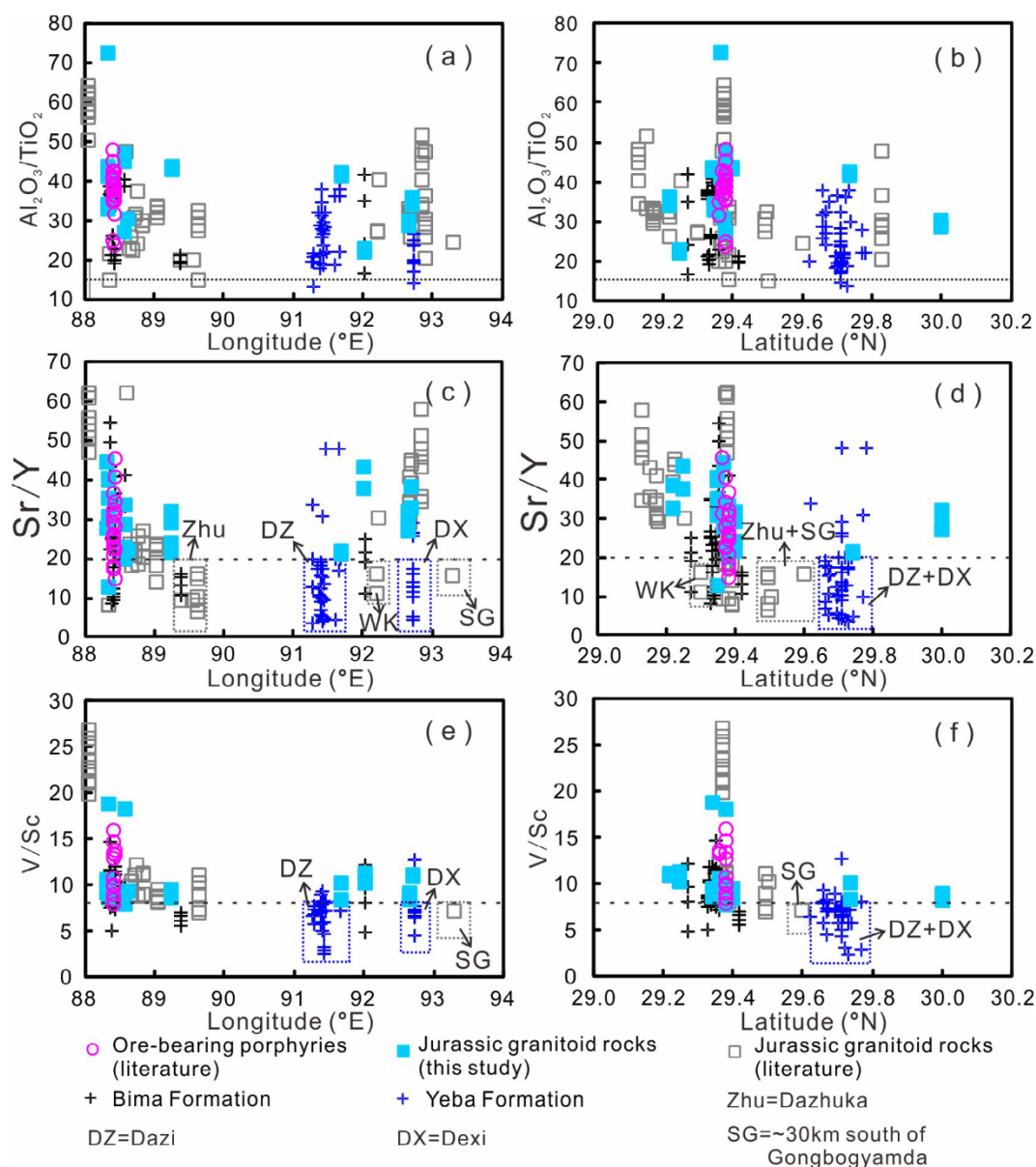


Fig. 13. Along-arc and across-arc whole-rock geochemical variations of the Jurassic magmatic rocks: (a) $\text{Al}_2\text{O}_3/\text{TiO}_2$ vs. Longitude; (b) $\text{Al}_2\text{O}_3/\text{TiO}_2$ vs. Latitude; (c) Sr/Y vs. Longitude; (d) Sr/Y vs. Latitude; (e) V/Sc vs. Longitude; (f) V/Sc vs. Latitude. Data sources are the same as for Fig. 4.

characteristics. In the future, further systematic isotopic studies on these magmatic rocks and more detailed information on the regional geology are required to establish the causes for the local anomalies more precisely.

7.4. Implication for porphyry copper mineralization in the Gangdese belt

Previous studies suggest that the fertility of Jurassic arc magmas exhibit spatial differences in the Gangdese belt (fertile western Gangdese belt and infertile eastern Gangdese belt, Hou et al., 2015b; fertile southern Gangdese belt and infertile northern Gangdese belt, Wang et al., 2017a). Our new data together with all of the published data show that Jurassic arc magmas in the whole Gangdese belt are generally water-rich and oxidized, except some local anomalous areas. Therefore, the whole Jurassic Gangdese arc belt is generally fertile rather than having systematic spatial fertility differences along the W-E or N-S trends. The rarity of the Jurassic subduction-related porphyry Cu deposit may be due to the varying degrees of erosion, or insufficient exploration in the Gangdese belt. Some Cretaceous and Cenozoic basins

have developed in the south of the Gangdese belt, and the clastic sediment in these basins could be derived from the Gangdese batholith (such as the Xigaze forearc basin; Wang et al., 2017c). Therefore, if the subduction-related porphyry Cu-Au deposits were eroded away, these Cretaceous and Cenozoic basins would be target regions to find ancient placer gold deposits. On the other hand, if many subduction-related porphyry Cu-Au deposits still exist, there is a large possibility that they were buried by volcano-sedimentary rocks. Therefore, the future exploration targets will be the fertile Jurassic volcanic rocks (such as Jurassic Bima Formation; Chen et al., 2019), and the Cretaceous and Cenozoic volcano-sedimentary rocks, if these rocks covered the subduction-related porphyry Cu deposits.

8. Conclusions

A comprehensive zircon U-Pb, trace element, Hf isotopic, whole-rock major and trace element and Sr-Nd isotopic study of Jurassic granitoid rocks in the Gangdese belt, together with pre-existing published data, has generated the following conclusions:

- (1) Our data show that the Jurassic granitoid rocks formed from 171.6 ± 1.1 to 195.3 ± 1.3 Ma, consistent with pre-existing published data.
- (2) The Jurassic granitoid rocks in the Gangdese belt are typical of arc-related rocks that formed by the interaction of mantle-wedge-derived basaltic magmas and juvenile lower crust, and underwent crystal fractionation.
- (3) The Jurassic arc magmas in the Gangdese belt are generally water-rich and oxidized, which are fertile for porphyry Cu mineralization, except in some localized anomalous areas.
- (4) The lack of the Jurassic subduction-related porphyry Cu deposits in the Gangdese belt may result from subsequent erosion or insufficient exploration.

Acknowledgments

This research was funded by the second Tibetan Plateau Scientific Expedition and Research (SETP) (2019QZKK0807), the National Key R & D Program of China (2016YFC0600407) and the National Natural Science Foundation of China (41772065, 41502073). We would like to thank Xinyu Wang and Shenglin Sun for assistance during the major and trace element analyses, and Congyin Li for providing support during the zircon U-Pb dating. Jeremy P. Richards is thanked for reviewing the earlier version of this manuscript, and may you rest in peace. We are grateful to the editor and reviewers for their constructive comments. This is contribution No.IS-2759 from GIGCAS.

Appendix A. Supplementary data

Supplementary data to this article can be found online at <https://doi.org/10.1016/j.oregeorev.2019.103169>.

References

- Annen, C., Blundy, J., Sparks, R., 2006. The genesis of intermediate and silicic magmas in deep crustal hot zones. *J. Petrol.* 47 (3), 505–539.
- Ballard, J.R., Palin, M.J., Campbell, I.H., 2002. Relative oxidation states of magmas inferred from Ce(IV)/Ce(III) in zircon: application to porphyry copper deposits of northern Chile. *Contrib. Mineral. Petrol.* 144, 347–364.
- Black, L.P., Kamo, S.L., Allen, C.M., Aleinikoff, J.N., Davis, D.W., Korsch, R.J., Foudoulis, C., 2003. TEMORA 1: a new zircon standard for Phanerozoic U-Pb geochronology. *Chem. Geol.* 200, 155–170.
- Blichert-Toft, J., Albarede, F., 1997. The Lu-Hf isotope geochemistry of chondrites and the evolution of the mantle-crust system. *Earth Planet. Sci. Lett.* 148 (1–2), 243–258.
- Blisniuk, P.M., Hacker, B.R., Glodny, J., Ratschbacher, L., Bi, S.W., Wu, Z.H., McWilliams, M.O., Calvert, A., 2001. Normal faulting in central Tibet since at least 13.5 Myr ago. *Nature* 412, 628–632.
- Cao, M.J., Qin, K.Z., Li, G.M., Li, J.X., Zhao, J.X., Evans, N.J., Hollings, P., 2016. Tectono-magmatic evolution of Late Jurassic to Early Cretaceous granitoids in the west central Lhasa subterrane, Tibet. *Gondwana Res.* 39, 386–400.
- Chen, W., Ma, C.Q., Bian, Q.J., Hu, Y.Q., Long, T.C., Yu, S.L., Chen, D.M., Tu, J.H., 2009. Evidence from geochemistry and Zircon U-Pb geochronology of volcanic rocks of Yeba formation in Demingding area, the East of middle Gangdise. *Tibet. Geol. Sci. Techno. Inform.* 28, 31–40 (in Chinese with English abstract).
- Chen, W., Ma, C.Q., Song, Z.Q., Long, T.C., Xia, T.Q., Cai, L.Y., Wang, T., 2011. Subduction-related early Jurassic granodiorite in Xiaodasongdu, the south of middle Gangdise in Tibet: evidences from Zircon U-Pb geochronology and geochemistry. *Geol. Sci. Techno. Inform.* 30, 1–12 (in Chinese with English abstract).
- Chen, X.L., Richards, J.P., Liang, H.Y., Zou, Y.Q., Zhang, J., Huang, W.T., Ren, L., Wang, F.Y., 2019. Contrasting arc magma fertilities in the Gangdese belt, Southern Tibet: evidence from geochemical variations of Jurassic volcanic rocks. *Lithos* 324–325, 789–802.
- Chu, M.F., Chung, S.L., Song, B., Liu, D., O'Reilly, S.Y., Pearson, N.J., Ji, J., Wen, D.J., 2006. Zircon U-Pb and Hf isotope constraints on the Mesozoic tectonics and crustal evolution of southern Tibet. *Geology* 34, 745–748.
- Coleman, M., Hodges, K., 1995. Evidence for Tibetan Plateau uplift before 14-myrs ago from a new minimum age for east-west extension. *Nature* 374, 49–52.
- Cooke, D.R., 2005. Giant porphyry deposits: characteristics, distribution, and tectonic controls. In: Cooke, D.R., Hollings, P., Walshe, J.L. (Eds.), *Giant Porphyry Deposits: Characteristics, Distribution, and Tectonic Controls*. Economic Geology, pp. 801–818.
- Dong, X., Zhang, Z.M., 2013. Genesis and tectonic significance of the Early Jurassic magmatic rocks from the southern Lhasa terrane. *Acta Petrol. Sin.* 29, 1933–1948.
- Dilles, J.H., Kent, A.J.R., Wooden, J.L., Tosdal, R.M., Koleszar, A., Lee, R.G., Farmer, L.P., 2015. Zircon compositional evidence for sulfur-degassing from ore-forming arc magmas. *Econ. Geol.* 110, 241–251.
- Ferry, J.M., Watson, E.B., 2007. New thermodynamic models and revised calibrations for the Ti-in-zircon and Zr-in-rutile thermometers. *Contrib. Mineral. Petrol.* 154, 429–437.
- Goto, A., Tatsumi, Y., 1994. Quantitative analysis of rock samples by an X-ray fluorescence spectrometer (I). *Rigaku J.* 11, 40–59.
- Griffin, W.L., Pearson, N.J., Belousova, E., Jackson, S.E., van Achterbergh, E., O'Reilly, S.Y., Shee, S.R., 2000. The Hf isotope composition of cratonic mantle: LAM-MC-ICPMS analysis of zircon megacrysts in kimberlites. *Geochim. Cosmochim. Acta* 64 (1), 133–147.
- Griffin, W.L., Wang, X., Jackson, S.E., Pearson, N.J., O'Reilly, S.Y., Xu, X.S., Zhou, X.M., 2002. Zircon chemistry and magma mixing, SE China: in-situ analysis of Hf isotopes, Tonglu and Pingtan igneous complexes. *Lithos* 61 (3–4), 237–269.
- Guan, Q., Zhu, D.C., Zhao, Z.D., Zhang, L.L., Liu, M., Li, X.W., Yu, F., Mo, X.X., 2010. Late Cretaceous adakites in the eastern segment of the Gangdese Belt, southern Tibet: products of Neo-Tethyan ridge subduction? *Acta Petrol. Sin.* 26 (7), 2165–2179 (in Chinese with English abstract).
- Guan, Q., Zhu, D.C., Zhao, Z.D., Dong, G.C., Mo, X.X., Liu, Y.S., Hu, Z.C., Yuan, H.L., 2011. Zircon U-Pb chronology, geochemistry of the Late Cretaceous mafic magmatism in the southern Lhasa Terrane and its implications. *Acta Petrol. Sin.* 27 (7), 2083–2094 (in Chinese with English abstract).
- Guo, L., Liu, Y., Liu, S., Cawood, P.A., Wang, Z., Liu, H., 2013. Petrogenesis of Early to Middle Jurassic granitoid rocks from the Gangdese belt, Southern Tibet: implications for early history of the Neo-Tethys. *Lithos* 179, 320–333.
- Hawkesworth, C.J., Turner, S.P., McDermott, F., Peate, D.W., Van Calsteren, P., 1997. U-Th isotopes in arc magmas: implications for element transfer from the subducted crust. *Science* 276, 551–555.
- Harlov, D., Tropper, P., Wolfgang, S., Timo, N., Forster, H.J., 2006. Formation of Al-rich titanite (CaTiSiO₄O-CaAlSiO₄OH) reaction rims on ilmenite in metamorphic rocks as a function of H₂O and fO₂. *Lithos* 88 (1–4), 72–84.
- Hildreth, W., Moorbath, S., 1988. Crustal contributions to arc magmatism in the Andes of central Chile. *Contrib. Mineral. Petrol.* 98, 455–489.
- Hou, Z., Duan, L., Lu, Y., Zheng, Y., Zhu, D., Yang, Z., Wang, B., Pei, Y., Zhao, Z., 2015a. Lithospheric architecture of the Lhasa terrane and its control on ore deposits in the Himalayan-Tibetan Orogen. *Econ. Geol.* 110, 1541–1575.
- Hou, Z., Yang, Z., Lu, Y., Kemp, A., Zheng, Y., Li, Q., Tang, J., Yang, Z., Duan, L., 2015b. A genetic linkage between subduction- and collision-related porphyry Cu deposits in continental collision zones. *Geology* 43, 643–650.
- Huang, W.T., Li, J., Liang, H.Y., Wang, C.L., Lin, S.P., Wang, X.Z., 2013. Zircon LA-ICP-MS U-Pb ages and highly oxidized features of magma associated with Luoboling porphyry Cu-Mo deposit in Zijinshan ore field, Fujian Province. *Acta Petrol. Sin.* 29, 283–293 (in Chinese with English abstract).
- Huang, W.T., Liang, H.Y., Wu, L., Wu, J., Li, J., Bao, Z.W., 2018. Asynchronous formation of the adjacent epithermal Au-Cu and porphyry Cu-Mo deposits in the Zijinshan orefield, southeast China. *Ore Geol. Rev.* 102, 351–367.
- Huang, Y., Tang, J.X., Lang, X.H., Zhang, L., Chen, Y., 2011. Geochemical characteristics of intrusive and volcanic rocks in No.II ore body of Xiongcu copper-gold deposit, Tibet: constraints on rock genesis and tectonic setting. *Mineral. Depos.* 30, 361–373 (in Chinese with English abstract).
- Huang, Y., Tang, J.X., Zhang, L., Lang, X.H., 2014a. Zircon U-Pb dating and Hf isotopic and trace element composition of intrusions from No.III orebody of Xiongcu porphyry copper-gold deposit, Tibet. *Mineral. Depos.* 33, 361–372 (in Chinese with English abstract).
- Huang, Y., Tang, J., Zhang, L., Lang, X., Center, C., 2014b. Zircon Hf isotopic composition of volcanic-magmatic rocks at Xiongcu porphyry copper-gold deposit, Tibet. *Acta Geol. Sin.* 88, 1528–1538 (in Chinese with English abstract).
- Ji, W.Q., Wu, F.Y., Chung, S.L., Li, J.X., Liu, C.Z., 2009. Zircon U-Pb geochronology and Hf isotopic constraints on petrogenesis of the Gangdese batholith, southern Tibet. *Chem. Geol.* 262, 229–245.
- Kang, Z.Q., Xu, J.F., Wilde, S.A., Feng, Z.H., Chen, J.L., Wang, B.D., Fu, W.C., Pan, H.B., 2014. Geochronology and geochemistry of the Sangri Group Volcanic Rocks, Southern Lhasa Terrane: implications for the early subduction history of the Neo-Tethys and Gangdese Magmatic Arc. *Lithos* 200, 157–168.
- Lang, X., Tang, J., Li, Z., Huang, Y., Ding, F., Yang, H., Xie, F., Zhang, L., Wang, Q., Zhou, Y., 2014. U-Pb and Re-Os geochronological evidence for the Jurassic porphyry metallogenetic event of the Xiongcu district in the Gangdese porphyry copper belt, southern Tibet, PRC. *J. Asian Earth Sci.* 79, 608–622.
- Le Maitre, R.W., Bateman, P., Dudek, A., Keller, J., Lameyre, J., Le Bas, M.J., Sabine, P.A., Schmid, R., Sorensen, H., Streckeisen, A., Woolley, A.R., Zanettin, B., 1989. *A Classification of Igneous Rocks and a Glossary of Terms*. International Union of Geosciences, Oxford, pp. 172.
- Li, X.H., Li, Z.X., Zhou, H.W., Liu, Y., Kinny, P.D., 2002. U-Pb zircon geochronology, geochemistry and Nd isotopic study of Neoproterozoic bimodal volcanic rocks in the Kangdian Rift of South China: implications for the initial rifting of Rodinia. *Precamb. Res.* 113, 135–154.
- Li, X.H., Qi, C.S., Liu, Y., Liang, X.R., Tu, X.L., Xie, L.W., Yang, Y.H., 2005. Petrogenesis of the Neoproterozoic bimodal volcanic rocks along the western margin of the Yangtze Block: new constraints from Hf isotopes and Fe/Mn ratios. *Chinese Sci. Bull.* 50 (21), 2481–2486.
- Li, X.H., Long, W.G., Li, Q.L., Liu, Y., Zheng, Y.F., Yang, Y.H., Chamberlain, K.R., Wan, D.F., Guo, C.H., Wang, X.C., Tao, H., 2010. Penglai Zircon Megacrysts: a potential new working reference material for microbeam determination of Hf-O isotopes and U-Pb Age. *Geostand. Geonanal. Res.* 34 (2), 117–134.
- Li, H., Zhang, H., Ling, M.X., Wang, F.Y., Ding, X., Zhou, J.B., Yang, X.Y., Tu, X.L., Sun, W.D., 2011. Geochemical and zircon U-Pb study of the Huangmeijian A-type granite: implications for geological evolution of the Lower Yangtze River belt. *Int. Geol. Rev.* 53, 499–525.

- Liang, X., Wei, G., Li, X., Liu, Y., 2003. Precise measurement of $^{143}\text{Nd}/^{144}\text{Nd}$ and Sm/Nd ratios using multiple-collectors inductively coupled plasma-mass spectrometer (MC-ICPMS). *Geochimica* 32 (1), 91–96 (in Chinese with English abstract).
- Liang, H.Y., Campbell, I.H., Allen, C., Sun, W.D., Liu, C.Q., Yu, H.X., Xie, Y.W., Zhang, Y.Q., 2006. Zircon $\text{Ce}^{4+}/\text{Ce}^{3+}$ ratios and ages for Yulong ore-bearing porphyries in eastern Tibet. *Miner. Deposita* 41, 152–159.
- Liang, H.Y., Sun, W.D., Su, W.C., Zartman, R.E., 2009. Porphyry Copper-Gold mineralization at Yulong, China, promoted by decreasing redox potential during magnetite alteration. *Econ. Geol.* 104, 587–596.
- Liu, Y., Hu, Z., Gao, S., Guenther, D., Xu, J., Gao, C., Chen, H., 2008. In situ analysis of major and trace elements of anhydrous minerals by LA-ICP-MS without applying an internal standard. *Chem. Geol.* 257 (1–2), 34–43.
- Liu, Z.C., Ding, L., Zhang, L.Y., Wang, C., Qiu, Z.L., Wang, J.G., Shen, X.L., Deng, X.Q., 2018. Sequence and petrogenesis of the Jurassic volcanic rocks (Yeba Formation) in the Gangdese arc, southern Tibet: implications for the Neo-Tethyan subduction. *Lithos* 312–313, 72–88.
- Loucks, R.R., 2014. Distinctive composition of copper-ore-forming arc magmas. *Aust. J. Earth Sci.* 61, 5–16.
- Ludwig, K.R., 2003. User's Manual for Isoplot 3.00: A Geochronological Toolkit for Microsoft Excel. Berkeley Geochronology Centre Special Publication, California.
- Lu, Y.J., Loucks, R.R., Fiorentini, M., McCuaig, T.C., Evans, N.J., Yang, Z.M., Hou, Z.Q., Kirkland, C.L., Parra-Avila, L.A., Kobussen, A., 2016. Zircon compositions as a pathfinder for porphyry Cu \pm Mo \pm Au deposits. *Econ. Geol.* 329–347.
- Wones, D.R., 1989. Significance of the assemblage titanite + magnetite + quartz in granitic rocks. *Am. Mineral.* 74, 744–749.
- Ma, X., Xu, Z., Meert, J., Santosh, M., 2017a. Early Jurassic intra-oceanic arc system of the Neotethys ocean: constraints from andesites in the Gangdese magmatic belt, south Tibet. *Island Arc*, e12202.
- Ma, X., Xu, Z., Chen, X., Meert, J.G., He, Z., Liang, F., Meng, Y., Ma, S., 2017b. The origin and tectonic significance of the volcanic rocks of the Yeba formation in the Gangdese Magmatic Belt, South Tibet. *J. Earth Sci.* 28 (2), 265–282.
- Mahoney, J.J., Frei, R., Tejada, M.L.G., Mo, X.X., Leat, P.T., Nägler, T.F., 1998. Tracing the Indian Ocean mantle domain through time: isotopic results from old West Indian, East Tethyan, and South Pacific seafloor. *J. Petrol.* 39, 1285–1306.
- Maniar, P.D., Piccoli, P.M., 1989. Tectonic discrimination of granitoids. *Geol. Soc. Am. Bull.* 101 (5), 635–643.
- Meng, Y.K., Dong, H.W., Cong, Y., Xu, Z.Q., Cao, H., 2016. The early-stage evolution of the Neo-Tethys ocean: Evidence from granitoids in the middle Gangdese batholith, southern Tibet. *J. Geodyn.* 94–95, 34–49.
- McDowell, S.M., Miller, C.F., Mundil, R., Ferguson, C.A., Wooden, J.L., 2014. Zircon evidence for a \sim 200 k.y. supereruption-related thermal flare-up in the Miocene southern Black Mountains, western Arizona, USA. *Contrib. Mineral. Petrol.* 168 (1031), 21.
- Pearce, J.A., Peate, D.W., 1995. Tectonic implications of the composition of volcanic arc magmas. *Annu. Rev. Earth Planet. Sci. Lett.* 23, 251–286.
- Pearce, N.J.G., Perkins, W.T., Westgate, J.A., Gorton, M.P., Jackson, S.E., Neal, C.R., Chener, S.P., 1997. A compilation of new and published major and trace element data for NIST SRM 610 and NIST SRM 612 glass reference materials. *Geostand. Newslett. J. Geostand. Geoanal.* 21, 115–144.
- Qiu, J.S., Wang, R.Q., Zhao, J.L., Yu, S.B., 2015. Petrogenesis of the Early Jurassic gabbro-granite complex in the middle segment of the Gangdese belt and its implications for tectonic evolution of Neo-Tethys: a case study of the Dongga pluton in Xi' gaze. *Acta Petrol. Sin.* 31 (12), 3569–3580 (in Chinese with English abstract).
- Qu, X., Xin, H., Xu, W., 2007. Petrogenesis of the ore-hosting volcanic rocks and their contribution to mineralization in Xiongcu superlarge Cu–Au deposit, Tibet. *Acta Geol. Sin.* 81, 964–971.
- Richards, J.P., 2003. Tectono-magmatic precursors for porphyry Cu(Mo–Au) deposit formation. *Econ. Geol.* 98 (8), 1515–1533.
- Richards, J.P., 2013. Giant ore deposits form by optimal alignments and combinations of geological processes. *Nat. Geosci.* 6, 911–916.
- Richards, J.P., 2015. The oxidation state, and sulfur and Cu contents of arc magmas: implications for metallogeny. *Lithos* 233, 27–45.
- Rickwood, P.C., 1989. Boundary lines within petrologic diagrams which use oxides of major and minor elements. *Lithos* 22, 247–263.
- Shui, X.F., He, Z.Y., Zhang, Z.M., Lu, T.Y., 2016. Magma Origin of Early Jurassic Tonalites in the Eastern Gangdese magmatic belt, Southern Tibet and its implications for the crustal evolution of the Lhasa Terrane. *Acta Geol. Sin.* 90 (11), 3129–3152.
- Shui, X.F., He, Z.Y., Klemd, R., Zhang, Z.M., Lu, T.Y., Yan, L.L., 2017. Early Jurassic adakitic rocks in the southern Lhasa sub-terrane, southern Tibet: petrogenesis and geodynamic implications. *Geol. Magaz.* 1–17.
- Sillitoe, R.H., 2010. Porphyry copper systems. *Econ. Geol.* 105, 3–41.
- Soderlund, U., Patchett, J.P., Vervoort, J.D., Isachsen, C.E., 2004. The Lu-176 decay constant determined by Lu-Hf and U-Pb isotope systematics of Precambrian mafic intrusions. *Earth Planet. Sci. Lett.* 219 (3–4), 311–324.
- Sun, S.S., McDonough, W.S., 1989. Chemical and isotopic systematics of oceanic basalts: implications for mantle composition and processes. *Geol. Soc. London Special Publ.* 42, 313–345.
- Sun, W.D., Liang, H.Y., Ling, M.X., Zhan, M.Z., Ding, X., Zhang, H., Yang, X.Y., Li, Y.L., Ireland, T.R., Wei, Q.R., 2013. The link between reduced porphyry copper deposits and oxidized magmas. *Geochim. Cosmochim. Acta* 103, 263–275.
- Sun, W.D., Huang, R.F., Li, H., Hu, Y.B., Zhang, C.C., Sun, S.J., Zhang, L.P., Ding, X., Li, C.Y., Zartman, R.E., 2015. Porphyry deposits and oxidized magmas. *Ore Geol. Rev.* 65, 97–131.
- Tafti, R., Mortensen, J.K., Lang, J.R., Rebagliati, M., Oliver, J.L., 2009. Jurassic U-Pb and Re-Os ages for the newly discovered Xietongmen Cu-Au porphyry district, Tibet, PRC: implications for metallogenic epochs in the southern Gangdese belt. *Econ. Geol.* 104, 127–136.
- Tafti, R., 2011. Unpublished Ph.D. thesis In: Metallogeny, Geochronology and Tectonic Setting of the Gangdese Belt, Southern Tibet, China. University of British Columbia, British Columbia, Canada, pp. 451.
- Tafti, R., Lang, J.R., Mortensen, J.K., Oliver, J.L., Rebagliati, C.M., 2014. Geology and geochronology of the Xietongmen (Xiongcu) Cu-Au Porphyry District, Southern Tibet, China. *Econ. Geol.* 109 (7), 1967–2001.
- Tang, J., Li, F., Li, Z., Zhang, L., Tang, X., Deng, Q., Lang, X., Huang, Y., Yao, X., Wang, Y., 2010. Time limit for formation of main geological bodies in Xiongcu copper-gold deposit, Xietongmen County, Tibet: Evidence from zircon U-Pb ages and Re-Os age of molybdenite. *Mineral. Depos.* 29 (3), 461–475 (in Chinese with English abstract).
- Tang, J., Lang, X., Xie, F., Gao, Y., Li, Z., Huang, Y., Ding, F., Yang, H., Zhang, L., Wang, Q., Zhou, Y., 2015. Geological characteristics and genesis of the Jurassic No. 1 porphyry Cu-Au deposit in the Xiongcu district, Gangdese porphyry copper belt, Tibet. *Ore Geol. Rev.* 70, 438–456.
- Wang, R., Richards, J.P., Hou, Z.Q., Yang, Z.M., Gou, Z.B., Dufrane, S.A., 2014a. Increasing magmatic oxidation state from paleocene to miocene in the Eastern Gangdese Belt, Tibet: implication for collision-related porphyry Cu-Mo \pm Au mineralization. *Econ. Geol.* 109, 1943–1965.
- Wang, R., Richards, J.P., Hou, Z.Q., Yang, Z.M., Dufrane, S.A., 2014b. Increased magmatic water content-the key to oligo-miocene porphyry Cu-Mo \pm Au formation in the Eastern Gangdese Belt, Tibet. *Econ. Geol.* 109, 1315–1339.
- Wang, R., Tafti, R., Hou, Z.Q., Shen, Z.C., Guo, N., Evans, N.J., Jeon, H., Li, Q.Y., Li, W.K., 2017a. Across-arc geochemical variation in the Jurassic magmatic zone, Southern Tibet: implication for continental arc-related porphyry Cu-Au mineralization. *Chem. Geol.* 451, 116–134.
- Wang, R.Q., Qiu, J.S., Yu, S.B., Zhao, J.L., 2017b. Crust-mantle interaction during Early Jurassic subduction of Neo-Tethyan oceanic slab: evidence from the Dongga gabbro-granite complex in the southern Lhasa subterrane, Tibet. *Lithos* 292, 262–277.
- Wang, J.G., Hu, X., Garzanti, E., An, W., Liu, X.C., 2017c. The birth of the Xigaze Forearc Basin in Southern Tibet. *Earth Planet. Sci. Lett.* 465, 38–47.
- Wen, D.R., Chung, S.L., Song, B., Iizuka, Y., Yang, H.J., Ji, J., Liu, D., Gallet, S., 2008a. Late Cretaceous Gangdese intrusions of adakitic geochemical characteristics, SE Tibet: petrogenesis and tectonic implications. *Lithos* 105 (1–2), 1–11.
- Wen, D.R., Liu, D., Chung, S.L., Chu, M.F., Ji, J., Zhang, Q., Song, B., Lee, T.Y., Yeh, M.W., Lo, C.H., 2008b. Zircon SHRIMP U-Pb ages of the Gangdese Batholith and implications for Neotethyan subduction in southern Tibet. *Chem. Geol.* 252 (3–4), 191–201.
- Wu, F.Y., Yang, Y.H., Xie, L.W., Yang, J.H., Xu, P., 2006. Hf isotopic compositions of the standard zircons and baddeleyites used in U-Pb geochronology. *Chem. Geol.* 234 (1), 105–126.
- Xie, F., Tang, J., Lang, X., Ma, D., 2018a. The different sources and petrogenesis of Jurassic intrusive rocks in the southern Lhasa subterrane, Tibet: evidence from the trace element compositions of zircon, apatite, and titanite. *Lithos* 314, 447–462.
- Xie, F.W., Tang, J.X., Chen, Y.C., Lang, X.H., 2018b. Apatite and zircon geochemistry of Jurassic porphyries in the Xiongcu district, southern Gangdese porphyry copper belt: implications for petrogenesis and mineralization. *Ore Geol. Rev.* 96, 98–114.
- Xu, B., Hou, Z.Q., Zheng, Y.C., Wang, R., He, M.Y., Zhou, L.M., Wang, Z.X., He, W.Y., Zhou, Y., Yang, Y., 2017a. In situ elemental and isotopic study of diorite intrusions: implication for Jurassic arc magmatism and porphyry Cu-Au mineralization in southern Tibet. *Ore Geol. Rev.* 90, 1063–1077.
- Xu, B., Hou, Z., Zheng, Y., Zhou, Y., Zhou, L., Yang, Y., Han, Y., Zhen, G., Wu, C., 2017b. Jurassic hornblende gabbros in Dongga, eastern Gangdese, Tibet: partial melting of mantle wedge and implications for crustal growth. *Acta Geol. Sin.* 91 (2), 545–564.
- Xu, J.F., Castillo, P.R., 2004. Geochemical and Nd–Pb isotopic characteristics of the Tethyan asthenosphere: implications for the origin of the Indian Ocean mantle domain. *Tectonophysics* 393, 9–27.
- Yang, Z.M., Hou, Z.Q., Jiang, Y.F., Zhang, H.R., Song, Y.C., 2011. Sr–Nd–Pb and zircon Hf isotopic constraints on petrogenesis of the Late Jurassic granitic porphyry at Qulong, Tibet. *Acta Petrol. Sin.* 27 (7), 2003–2010 (in Chinese with English abstract).
- Yin, A., Harrison, T.M., 2000. Geologic evolution of the Himalayan-Tibetan orogen. *Annu. Rev. Earth Planet. Sci. Lett.* 28, 211–280.
- Yin, Q., Lang, X., Cui, Z., Yang, Z., Xie, F., Wang, X., 2017. Geology and geochemistry constraints on the genesis of the No. 2 porphyry copper-gold deposit in the Xiongcu district, Gangdese porphyry copper belt, Tibet, China. *Appl. Ecol. Environ. Res.* 15 (3), 477–508 (in Chinese with English abstract).
- Zhang, S.Q., Mahoney, J.J., Mo, X.X., Ghazi, A.M., Milani, L., Crawford, A.J., Guo, T.Y., Zhao, Z.D., 2005. Evidence for a widespread Tethyan upper mantle with Indian-Ocean type isotopic characteristics. *J. Petrol.* 46, 829–858.
- Zhang, R.F., Xu, W.C., Guo, J.Q., Zong, K.Q., Cai, H.M., Yuan, H.L., 2007. Zircon U-Pb and Hf isotopic composition of deformed granite in the southern margin of the Gangdese belt, Tibet: evidence for early Jurassic subduction of Neo-Tethyan oceanic slab. *Acta Petrol. Sin.* 23 (6), 1347–1353.
- Zhang, L., Ren, Z.Y., Nichols, A.R.L., Zhang, Y.H., Zhang, Y., Qian, S.P., Liu, J.Q., 2014a. Lead isotope analysis of melt inclusions by LA-MC-ICP-MS. *J. Anal. Atomic Spectrom.* 29 (8), 1393–1405.
- Zhang, Z.M., Dong, X., Xiang, H., He, Z., Liou, J.G., Santosh, M., 2014b. Metagabbros of the Gangdese arc root, south Tibet: implications for the growth of continental crust. *Geochim. Cosmochim. Acta* 143, 268–284.
- Zhang, L., Ren, Z.Y., Xia, X.P., Li, J., Zhang, Z.F., 2015. IsotopeMaker: a Matlab program for isotopic data reduction. *Int. J. Mass Spectrom.* 392, 118–124.
- Zhu, D.C., Pan, G.T., Chung, S.L., Liao, Z.L., Wang, L.Q., Li, G.M., 2008. SHRIMP zircon age and geochemical constraints on the origin of lower Jurassic volcanic rocks from the Yeba formation, Southern Gangdese, south Tibet. *Int. Geol. Rev.* 50, 442–471.
- Zhu, D., Zhao, Z., Niu, Y., Mo, X., Chung, S., Hou, Z., Wang, L., Wu, F., 2011. The Lhasa Terrane: record of a microcontinent and its histories of drift and growth. *Earth Planet. Sci. Lett.* 301, 241–255.

- Zhu, D.C., Wang, Q., Zhao, Z.D., Chung, S.L., Cawood, P.A., Niu, Y.L., Liu, S.A., Wu, F.Y., Mo, X.X., 2015. Magmatic record of India-Asia collision. *Sci. Rep.* 5, 14289.
- Zhu, D.C., Wang, Q., Cawood, P.A., Zhao, Z.D., Mo, X.X., 2017. Raising the Gangdese mountains in southern Tibet. *J. Geophys. Res.: Solid Earth* 122, 214–223.
- Zou, Y.Q., Huang, W.T., Liang, H.Y., Wu, J., Lin, S.P., Wang, X.Z., 2015. Identification of porphyry genetically associated with mineralization and its zircon U-Pb and biotite Ar-Ar age of the Xiongcu Cu-Au deposit, southern Gangdese, Tibet. *Acta Petrol. Sin.* 31, 2053–2062 (in Chinese with English abstract).
- Zou, Y.Q., Chen, X.L., Huang, W.T., Zhang, J., Liang, H.Y., Xu, J.F., Chen, L., 2017. Identification of an Early-Middle Jurassic oxidized magmatic belt, south Gangdese, Tibet, and geological implications. *Sci. Bulletin* 62, 888–898.